JCB Journal of Cell Biology

ARTICLE

SLX4–XPF mediates DNA damage responses to replication stress induced by DNA–protein interactions

Riko Ishimoto*, Yota Tsuzuki*, Tomoki Matsumura, Seiichiro Kurashige, Kouki Enokitani, Koki Narimatsu, Mitsunori Higa, Nozomi Sugimoto, Kazumasa Yoshida, and Masatoshi Fujita

The DNA damage response (DDR) has a critical role in the maintenance of genomic integrity during chromosome replication. However, responses to replication stress evoked by tight DNA–protein complexes have not been fully elucidated. Here, we used bacterial LacI protein binding to *lacO* arrays to make site-specific replication fork barriers on the human chromosome. These barriers induced the accumulation of single-stranded DNA (ssDNA) and various DDR proteins at the *lacO* site. SLX4–XPF functioned as an upstream factor for the accumulation of DDR proteins, and consequently, ATR and FANCD2 were interdependently recruited. Moreover, LacI binding in S phase caused underreplication and abnormal mitotic segregation of the *lacO* arrays. Finally, we show that the SLX4–ATR axis represses the anaphase abnormality induced by LacI binding. Our results outline a long-term process by which human cells manage nucleoprotein obstacles ahead of the replication fork to prevent chromosomal instability.

Introduction

Dysfunctional DNA replication ultimately causes genomic instability and development of many human diseases, including cancers (Lecona and Fernández-Capetillo, 2014; Zhang and Walter, 2014; Gaillard et al., 2015). Replication forks traveling along chromosomal DNA are often impaired by endogenous and exogenous sources of replication stress, such as collision with transcription complexes, proteins that are tightly bound to DNA, DNA lesions, repetitive DNA sequences, starvation of deoxynucleoside triphosphates, and oncogene activation (Kotsantis et al., 2018; Lambert and Carr, 2013; García-Muse and Aguilera, 2016; Magdalou et al., 2014). In eukaryotic cells, harmful consequences such as deleterious chromosomal rearrangements are prevented by elaborate integrated pathways of DNA damage response (DDR) to diverse replication stresses (Muñoz and Méndez, 2017; Nickoloff et al., 2017; Hills and Diffley, 2014).

Among the DDR pathways, ATR (ataxia telangiectasia mutated and Rad3 related) is a central factor for maintenance of genomic integrity during DNA replication (Saldivar et al., 2017; Toledo et al., 2017). When DNA polymerases are halted, a functional uncoupling of the polymerase and replicative helicase occurs, leading to the accumulation of RPA (replication protein A)–bound single-stranded DNA (ssDNA), which serves as a platform for recruitment and activation of ATR by activator proteins TOPBP1 (DNA topoisomerase II binding protein 1) or ETAA1 (Ewing's tumor-associated antigen 1;Saldivar et al., 2017; Blackford and Jackson, 2017). ATR is also involved in the Fanconi anemia (FA) pathway, which is mainly activated by DNA interstrand crosslinks (ICLs; Ishiai et al., 2017; Michl et al., 2016). A key step of the FA pathway is monoubiquitination of FANCI (FA group I)–FANCD2 (FA group D2) heterodimeric (ID2) complexes by the FA core E3-ligase complex, followed by incision-dependent repair steps, including ICL unhooking, lesion bypass, homologous recombination, and nucleotide-excision repair (Duda et al., 2016; Niraj et al., 2019). The scaffold protein SLX4 (synthetic lethal of unknown function 4) interacts with structure-specific endonucleases such as XPF (xeroderma pigmentosum group F)–ERCC1 (excision repair cross-complementation group 1), MUS81 (methyl methanesulfonate and UV sensitive 81)–EME1 (essential meiotic endonuclease 1), and SLX1, and has a crucial role in the ICL-repair processes following ID2 monoubiquitination (Niraj et al., 2019; Zhang and Walter, 2014; Datta and Brosh, 2019). SLX4 also functions in the resolution of Holliday junctions and the maintenance of common fragile sites (Kim and Forsburg, 2018; Dehé and Gaillard,

Department of Cellular Biochemistry, Graduate School of Pharmaceutical Sciences, Kyushu University, Fukuoka, Japan.

*R. Ishimoto and Y. Tsuzuki contributed equally to this paper; Correspondence to Kazumasa Yoshida: kyoshida@phar.kyushu-u.ac.jp; Masatoshi Fujita: mfujita@phar.kyushu-u.ac.jp.

2017; Minocherhomji and Hickson, 2014). In addition, ATM (ataxia telangiectasia mutated) is activated at sites of DNA double-strand breaks (DSBs) and triggers DNA repair pathways and damage checkpoint signaling (Mladenov et al., 2016; Blackford and Jackson, 2017). A replication fork is converted into a DSB by a severe impediment to DNA replication or an encounter with a single-strand break on the template DNA (Syeda et al., 2014). Breakage of a replication fork may generate a one-ended DNA break, and homology-directed repair pathways and/or a converging replication fork would recover the broken fork (Ait Saada et al., 2018; Magdalou et al., 2014; Kramara et al., 2018; Helleday, 2003).

Although the DDR pathways that act in response to replication stresses induced experimentally via exogenous sources have been investigated, the mechanistic details of DDRs associated with replication interference at endogenous "difficult-to-replicate" regions remain to be clarified. In addition to replication–transcription conflict and abnormal DNA structures, large nucleoprotein structures can be features of such regions (Gadaleta and Noguchi, 2017; Mirkin and Mirkin, 2007). Protein binding to chromatin can act as a natural replication fork barrier in eukaryotic cells, as found at the ribosomal DNA array (Dalgaard et al., 2011). Tight interactions between repetitive DNA sequences and specific binding proteins would perturb fork progression at difficult-to-replicate regions, such as centromeres and telomeres, which are linked to chromosome fragility and recombinational hotspots (Sarlós et al., 2017; Salim and Gerton, 2019; Higa et al., 2017a; Black and Giunta, 2018).

To assess DDR induced by replication forks stalling at tight DNA–protein complexes, we employed an experimental model system using bacterial *lacO*–LacI interactions to recapitulate a site-specific replication fork barrier at *lacO* arrays stably integrated into the mammalian chromosome (Jacome and Fernandez-Capetillo, 2011; Beuzer et al., 2014; Kim et al., 2018). We investigated the spatiotemporal dynamics of accumulation of DDR proteins and identified novel SLX4-dependent DDR signaling at the difficult-to-replicate region. Our results also demonstrated that tight protein binding causes defective mitotic segregation of the *lacO* site, probably as a result of incomplete replication, and that the SLX4–ATR axis alleviates the anaphase abnormality. Although some findings for DDRs induced by *lacO*–LacI interactions have previously been reported (Jacome and Fernandez-Capetillo, 2011; Beuzer et al., 2014; Kim et al., 2018), our study has now provided a more comprehensive picture of a process by which human cells manage nucleoprotein obstacles ahead of replication forks to prevent chromosomal instability.

Results

A tight protein–DNA complex on a human chromosome induces replication stress responses during S phase

To induce LacI binding to *lacO*, we first transiently transfected a HA epitope–tagged LacI expression vector into asynchronous human U2OS 2-6-3 cells containing a 200-copy array of 256 *lacO* repeats in chromosome 1 (Janicki et al., 2004). At 24 h after transfection, fluorescence imaging demonstrated that various DDR proteins (including ATR, RPA, and FANCD2) had been recruited to *lacO* sites (Fig. S1 A). ChIP analysis further showed that binding of FANCD2 and TOPBP1 to *lacO* is specifically enhanced by LacI expression (Fig. S1 B). Furthermore, expression of LacI-induced RPA phosphorylation and FANCD2 monoubiquitination, as demonstrated by mobility shifts on SDS-PAGE (Anantha et al., 2007; Ishiai et al., 2017), as well as phosphorylation of Chk1 (checkpoint kinase 1; Fig. S1 C), indicating that LacI binding to the *lacO* arrays activates the ATR and FA pathways. Notably, these protein modifications were suppressed by the ATR/ATM-kinase inhibitor VE-821, which inhibited ATR, but not ATM, under the condition used here (Fig. S1, C and D).

We next established U2OS 40-2-6 cells expressing the estrogen receptor (ER)–based construct ER^{T2}-HA-LacI (ΔNLS), in which rapid LacI binding to *lacO* is induced by treatment with 4-OH-tamoxifen (4-OHT; Fig. 1 A). ChIP experiments using anti-LacI antibody further showed that in the absence of 4-OHT treatment, only a background level of LacI binds to *lacO* sequences, and 4-OHT treatment induces remarkable LacI binding (Fig. S2 C). In addition, the results of bromodeoxyuridine immunoprecipitation (BrdU-IP) assays showed that incorporation of BrdU at the *lacO* arrays is inhibited by treatment with 4-OHT, suggesting that LacI binding is an obstacle for progression of the replication fork (Fig. 1 B). As in the transiently transfected cells (Fig. S1), various DDR proteins were recruited to the LacI-bound locus 2 h after 4-OHT treatment (Fig. 1, C and D; and Fig. S2 A). We also found that components of the DSB signaling and repair pathway, including 53BP1 (p53-binding protein 1), phospho-ATM (p-ATM; Ser1981), and RAD52 (radiation sensitive 52), but not RAD51 (radiation sensitive 51), are associated with the *lacO* sites. ChIP analysis showed that LacI binding promotes accumulation of 53BP1 at *lacO* (Fig. S2 C). By immunofluorescence-based detection of BrdU-labeled DNA under nondenaturing conditions (Buisson et al., 2015), we found that ssDNA is extensively exposed at the LacI-bound *lacO* sites (Fig. 1 D and Fig. S2 A). Furthermore, by the use of distinct labeling methods to selectively detect nascent-strand or parental-strand ssDNA (Couch et al., 2013), we found that parental-strand ssDNA is preferentially exposed at the *lacO* sites (Fig. 1 D and Fig. S2 A).

Next, we examined the impacts of cell-cycle synchronization on the accumulation of DDR proteins. In G1-arrested or G0-arrested cells, the frequencies of colocalization of these proteins with the LacI focus were generally lower than in S-phase cells, although some accumulation of the DSB signaling and repair proteins p-ATM and 53BP1 was still observed in G1 cells (Fig. 1 E and Fig. S3), possibly as a result of underreplication of the *lacO* array (see below). Accumulation of ATR, RPA34, and FANCD2 was substantially enhanced upon release from hydroxyurea (HU)–mediated arrest in early S phase (Fig. S3 I). Taken together, these data indicate that the DDRs associated with the *lacO* array are induced upon blockage of fork progression by LacI binding.

Dynamic association of DDR factors to LacI-stalled replication forks in S phase involves SLX4–XPF early response and subsequent interdependent recruitment of ATR and FANCD2

We investigated the temporal dynamics of the accumulation of DDR factors to the LacI-bound *lacO* array in cells that had been

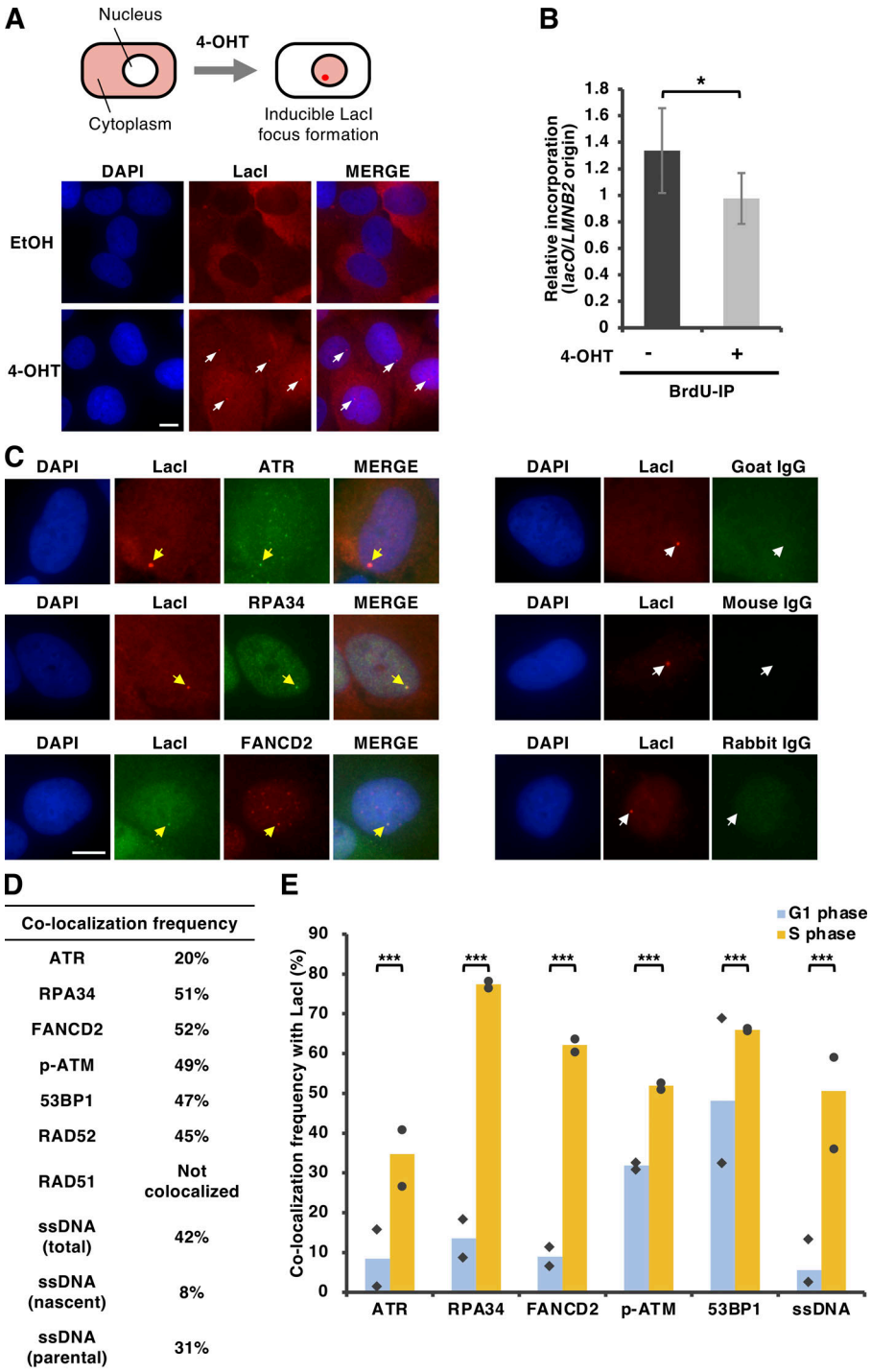

Figure 1. **Various DDR proteins are recruited to the LacI-bound *lacO* array in an S-phase–specific manner. (A)** A schematic is shown of the rapid and controlled induction of LacI binding to *lacO* in U2OS 40–2-6 cells stably expressing HA-ER^{T2}-LacI (ΔNLS). Nuclear accumulation of HA-ER^{T2}-LacI (ΔNLS) was stimulated by treatment with 4-OHT. Representative images are shown of U2OS 40–2-6 ER-LacI cells treated with 4-OHT or vehicle only (EtOH) for 30 min. LacI was detected with anti-LacI immunostaining (red) and DNA with DAPI staining (blue). White arrows indicate LacI foci. Scale bar, 10 µm. **(B)** U2OS 40–2-6 ER-LacI cells were treated with 1 µM 4-OHT or vehicle-only (EtOH) for 80 min and labeled with 10 µM BrdU for the last 20 min. BrdU incorporation was then examined by DNA immunoprecipitation with anti-BrdU antibody (BrdU-IP), followed by quantitative PCR analysis using primer pairs to detect the *lacO* sequences or *LMNB2* replication origin. The relative incorporation of BrdU into the *lacO* sequences compared with the control region (*LMNB2* origin) was calculated. The means ± SD are shown (n = 6). *, P < 0.05 (two-tailed Student's t test). **(C and D)** U2OS 40–2-6 ER-LacI cells treated with 1 µM 4-OHT for 2 h were double immunostained with the indicated antibodies and counterstained with DAPI. ssDNA was detected with anti-BrdU antibody under nondenaturing conditions. **(C)** Representative images are shown. Yellow and white arrows indicate colocalization and noncolocalization of DDR proteins with the LacI foci, respectively. Scale bar, 10 µm. **(D)** Colocalization frequencies of the indicated foci with the LacI foci are shown. Values were calculated from the sum scores of at least two independent experiments. **(E)** U2OS 40–2-6 ER-LacI cells were synchronized in G1 phase by lovastatin treatment or in S phase by HU treatment with subsequent release for 4 h (for details, see Materials and methods), then treated with 1 µM 4-OHT for 2 h and double immunostained, followed by DAPI staining and analysis. Colocalization frequencies were calculated from the sum scores of two independent experiments. ***, P < 0.001 (χ^2 test). Individual data points from the two experiments are also depicted.

released from HU arrest for 1–8 h and found that RPA accumulation at the array peaks ∼4–6 h after release, with accumulation of ATR and FANCD2 peaking 6–8 h after release (Fig. 2). Colocalization of p-ATM and 53BP1 with *lacO* peaked at 4 h, and the peak of RAD52 occurred at 6 h. In the accumulation of scaffold protein SLX4 and its associated nucleases (Kim and Forsburg, 2018), SLX4 and XPF persisted at high levels throughout the examined period of S phase, whereas colocalization of MUS81 decreased during the first 4 h, then increased to peak at 8 h. Colocalization of SLX1 gradually increased to peak at 8 h. SLX4 and XPF accumulated even in G1 phase (Fig. S3 E) and HU-arrested cells (Fig. S3 I), suggesting the possibility that part of SLX4–XPF is associated with the *lacO* as a difficult-to-replicate region independently of replication fork inhibition (for more details, see below).

To test the role of SLX4 in the replication stress response induced by LacI binding to *lacO*, expression of *SLX4* was knocked down by specific siRNAs (Fig. S4 A). We confirmed that knockdown of *SLX4* does not cause a reduction in the levels of XPF and MUS81 proteins (Fig. S4 A), in agreement with previous

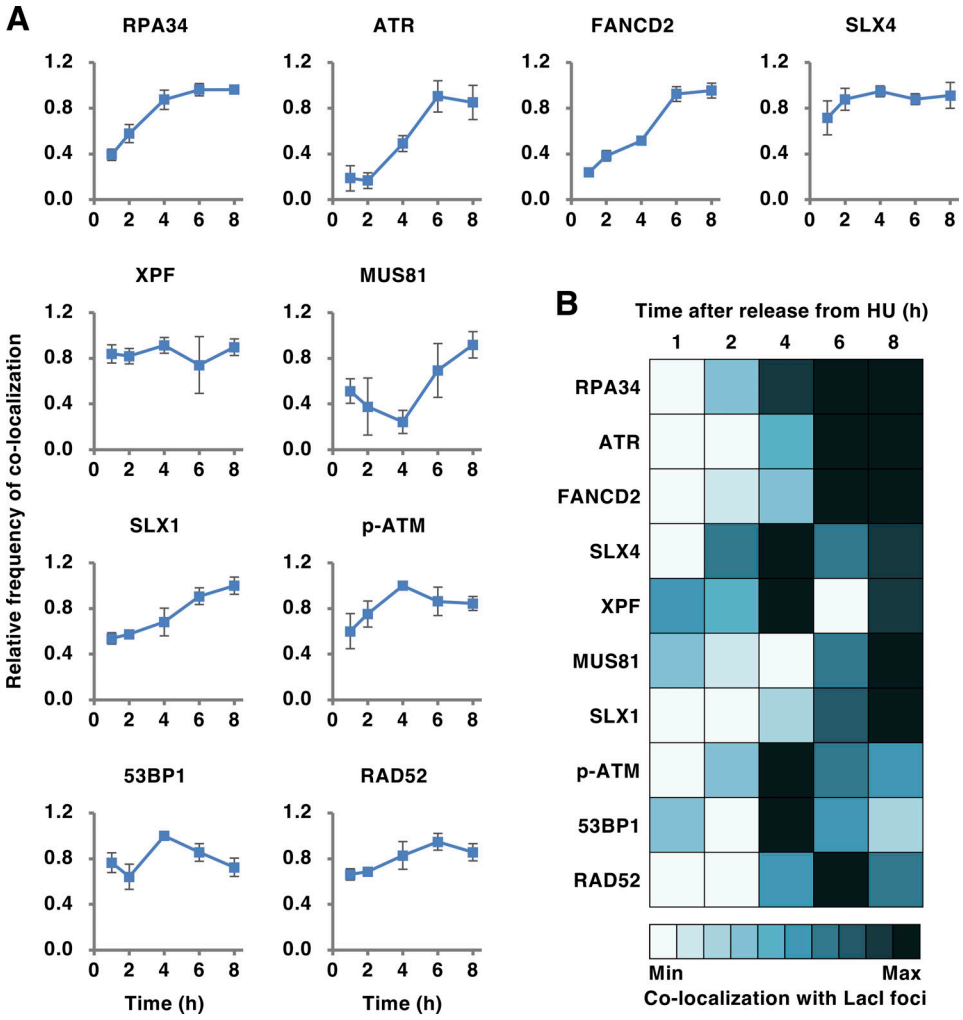

Figure 2. **DDR factors associated with ATR, FA, and ATM pathways accumulate at the LacI-bound *lacO* array with distinct dynamics. (A)** U2OS 40–2-6 ER-LacI cells were synchronized with 2.5 mM HU for 18 h and released into fresh medium containing 1 µM 4-OH-tamoxifen for the indicated times. Cells were then double immunostained with anti-LacI antibody and the indicated antibodies, followed by DAPI staining and analysis. Colocalization frequencies of the indicated foci with the LacI foci are shown, with maximum value of the colocalization frequency for each factor set at 1. Values depicted are means ± SD from three independent experiments. **(B)** The spatiotemporal heatmap depicts the accumulation kinetics of the DDR factors. The maximum–minimum range of the relative frequency of colocalization shown in (A) was calculated for each factor, then each range was equally divided into 10 fractions, which were assigned colors as indicated in the bottom panel.

findings (Panier et al., 2019; Sarbajna et al., 2014). As shown in Fig. 3 A and Fig. S4 B, *SLX4* knockdown reduced the accumulation of DDR proteins at the *lacO* array. In addition, knockdown experiments for SLX4-associated nucleases demonstrated that XPF, but not MUS81, is involved in the accumulation of RPA and ATR (Fig. 3, B and C; and Fig. S4, C–F). *XPF* knockdown neither reduced SLX4 and MUS81 protein levels (Fig. S4 C) nor impaired the accumulation of SLX1 (Fig. S4 D). In addition, *MUS81* knockdown did not reduce the SLX4 and XPF protein levels (Fig. S4 E). These results suggest that SLX4 and XPF act at an early stage of the response to generate ssDNA.

We also investigated the interactions between the ATR and FA pathways. *FANCD2* knockdown by siRNAs led to a significant reduction in the accumulation of ATR at *lacO* sites (Fig. 3 D; and Fig. S4, G and H). Inhibition of ATR-kinase activity by VE-821 significantly abrogated the accumulation of FANCD2, but not RPA (Fig. 3 E and Fig. S4 I). These results reveal that following SLX4 localization, ATR and FANCD2 are recruited interdependently to stalled replication forks.

Underreplication of the *lacO* array is prompted by, but not dependent upon, LacI binding in S phase

Upon replication stress, difficult-to-replicate regions such as common fragile sites occasionally cannot be fully duplicated during S phase (Debatisse and Rosselli, 2019). Such unreplicated regions undergo mitotic DNA repair synthesis (MiDAS) in early mitosis, and some regions remain underreplicated until the next cell cycle (Minocherhomji et al., 2015; Moreno et al., 2016; Spies et al., 2019; Özer and Hickson, 2018). Here, we investigated whether MiDAS is induced on the LacI-bound *lacO* array. As previously described (Minocherhomji et al., 2015), we used a Cdk1 (cyclin-dependent kinase 1) inhibitor (RO-3306) to synchronize U2OS 40–2-6 cell cycles at G2 phase, with or without 4-OHT, to test the influence of LacI binding during the preceding

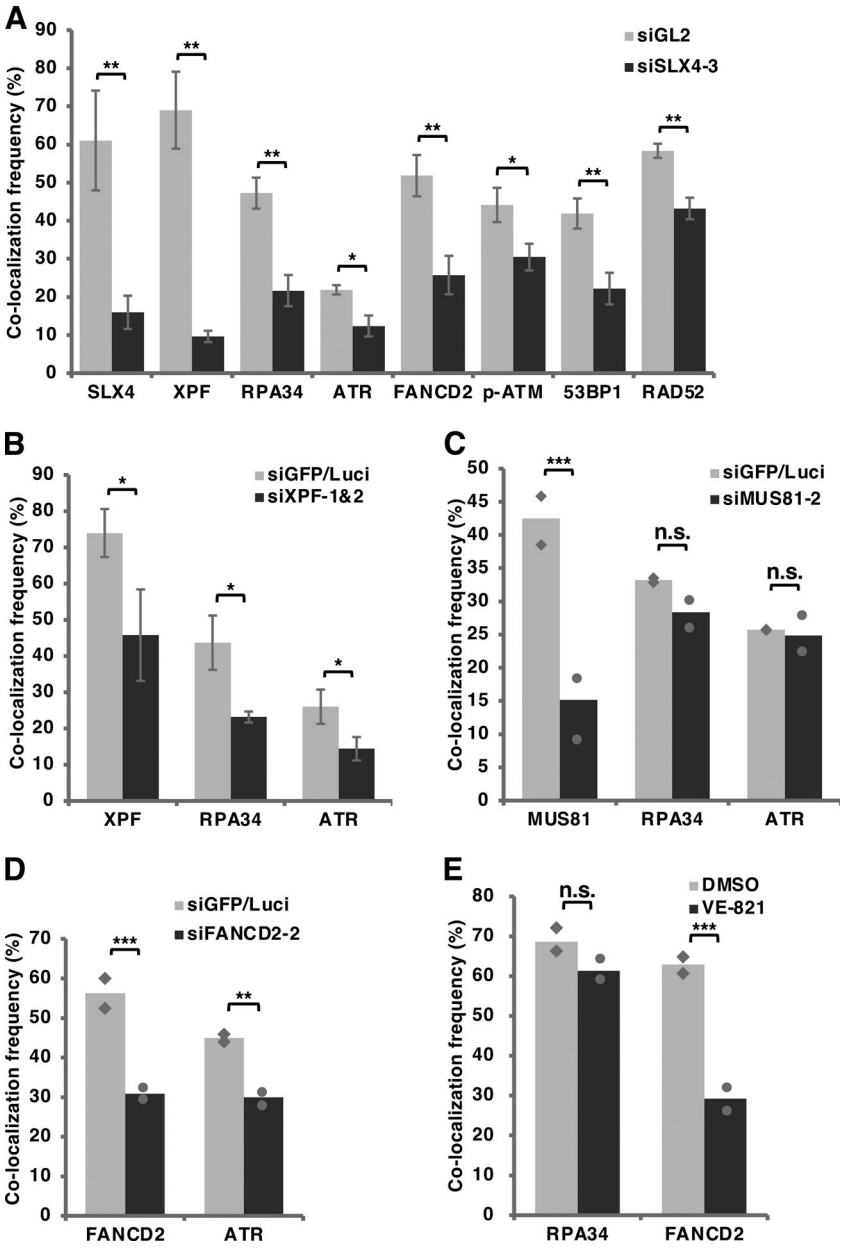

Figure 3. **Silencing of SLX4–XPF suppresses accumulation of DDR factors at *lacO*, and the subsequent accumulations of ATR and FANCD2 are interdependent. (A)** U2OS 40–2-6 ER-LacI cells were transfected with control (siGL2) or SLX4 (siSLX4-3)-targeting siRNAs for 48 h. The cells were further treated with 1 µM 4-OH-tamoxifen (4-OHT) for 2 h, then subjected to colocalization analysis by double immunostaining. Similar experiments using other siRNAs are shown in Fig. S4 B. **(B–D)** U2OS 40–2-6 ER-LacI cells were transfected with control (mixture of siGFP and siLuci) siRNAs or siRNAs targeting XPF (siXPF-1 and siXPF-2), MUS81 (siMUS81-2), or FANCD2 (siFANCD2-2) for 48 h. **(B and C)** Following siRNA treatment, cells were treated with 1 µM 4-OHT for 2 h and subjected to colocalization analysis. **(D)** At 42 h after siRNA transfection, cells were treated with 1 µM 4-OHT for 6 h and then analyzed. Similar experiments using other siRNAs are shown in Fig. S4, F and H. **(E)** U2OS 40–2-6 ER-LacI cells were treated with 10 µM ATR inhibitor (VE-821) or vehicle only (DMSO) for 6 h, with 1 µM 4-OHT for the last 2 h, followed by colocalization analysis. For A and B, the means ± SD from three independent experiments are shown. *, $P < 0.05$; **, $P < 0.01$ (two-tailed Student's *t* test). For C–E, the values were calculated from the sum scores of two independent experiments. **, $P < 0.01$; ***, $P < 0.001$; n.s., not significant (χ^2 test). Individual data points from the two independent experiments are also depicted.

S phase (Fig. 4, A and B). It has been proposed that FANCD2 and MUS81 accumulate at underreplicated regions in G2/M cells and protect genome stability (Chan et al., 2009; Naim et al., 2013; Ying et al., 2013; Minocherhomji et al., 2015; Duda et al., 2016). As shown in Fig. 4 C, colocalization of FANCD2 with LacI on prophase or prometaphase chromosomes was significantly greater in cells with than in those without LacI induction in S phase, suggesting that LacI binding contributes to underreplication of *lacO* repeats. However, 62.4% of prophase/prometaphase LacI foci showed colocalization with FANCD2 even in the absence of S-phase LacI, raising the possibility that the *lacO* repeat is intrinsically difficult to replicate and that it remains unreplicated regardless of S-phase LacI binding. MUS81 also accumulated on the mitotic *lacO* array, and S-phase LacI binding only slightly enhanced prophase/prometaphase colocalization (Fig. 4 D). In addition, we found that MiDAS, which occurs specifically in mitotic cells (not in G2-arrested cells), is activated at *lacO* even in the absence of S-phase LacI (Fig. 4, E–G). These data suggest that even in the absence of LacI binding, most early mitotic cells (~60%) contain underreplicated *lacO* arrays, and these lesions are repaired by MiDAS in only ~20% of the cells, leaving ~40% of cells with underreplicated *lacO* arrays (see Discussion and Fig. 8). With LacI binding in the preceding S phase, ~90% of early mitotic cells contain underreplicated *lacO* arrays, with a similar level of MiDAS repair, leaving ~70% of cells with underreplicated *lacO* arrays.

LacI binding in S phase induces aberrant segregation of the *lacO* array, and the SLX4–ATR axis prevents induction of anaphase abnormality by replication stress

Although MUS81-mediated cleavage of underreplicated chromosomes can induce MiDAS to complete the replication (Ying

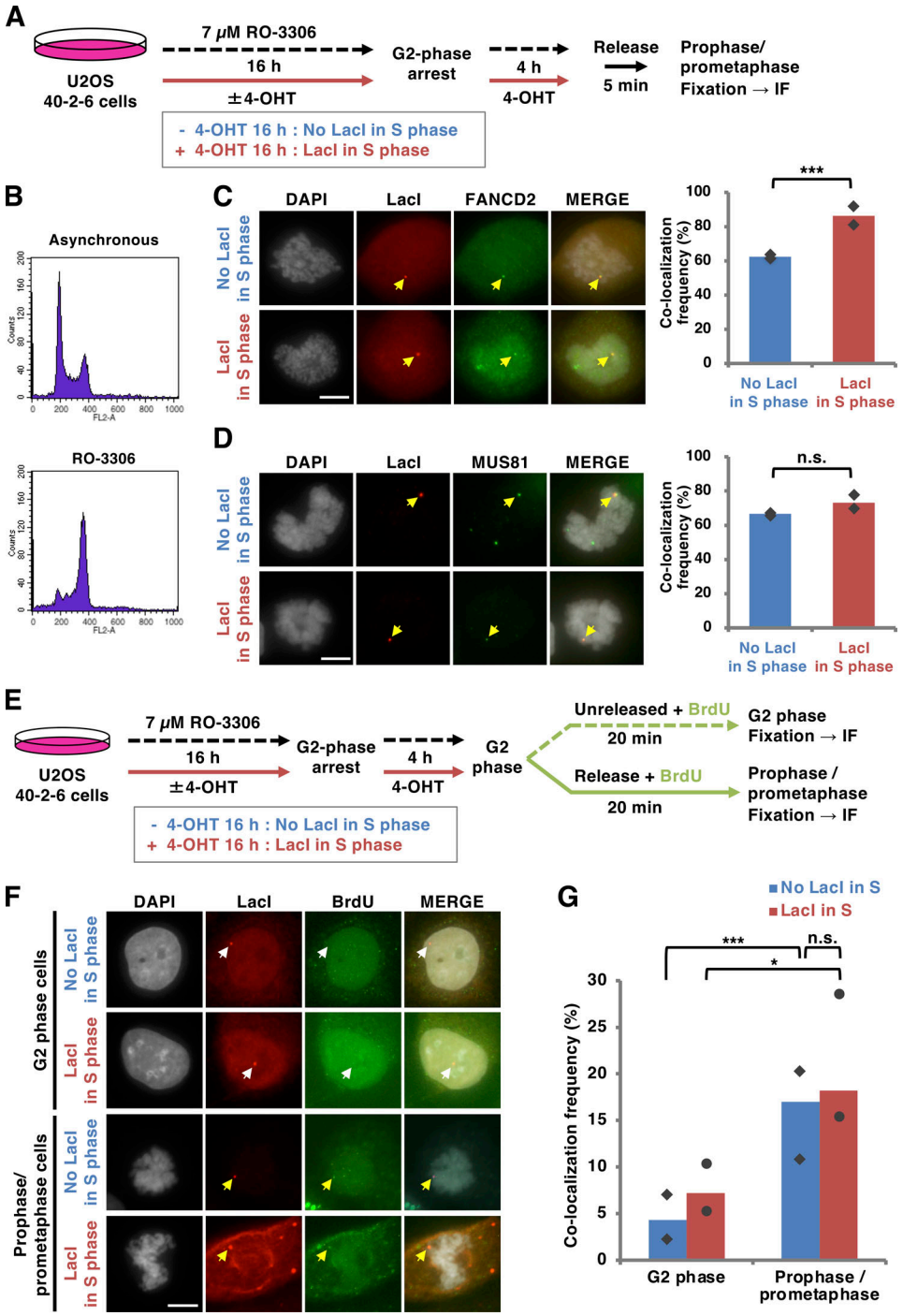

Figure 4. **FANCD2 and MUS81 accumulate on the *lacO* array in mitosis, where MiDAS is activated, and LacI binding during S phase increases FANCD2 colocalization with *lacO*. (A)** Experimental scheme. U2OS 40–2-6 ER-LacI cells were synchronized in late G2 phase with 7 μM RO-3306 treatment for 20 h and 1 μM 4-OHT for 20 h or the last 4 h. G2-arrested cells were then released into fresh medium for 5 min and subjected to double immunostaining, DAPI staining, and analysis. **(B)** Confirmation of G2-phase synchronization with RO-3306. U2OS 40–2-6 ER-LacI cells synchronized in G2 phase by incubation with 7 μM RO-3306 for 16 h were subjected to FACS analysis. **(C and D)** Representative images (left) and colocalization frequencies (right) are shown. Values were calculated from the sum scores of two independent experiments. ***, $P < 0.001$; n.s., not significant (χ^2 test). Individual data points from the two independent experiments are also shown. Yellow arrows indicate colocalization of FANCD2 (C) or MUS81 (D) with the LacI foci. Scale bars, 10 μm. **(E)** Experimental workflow for MiDAS detection. U2OS 40–2-6 ER-LacI cells were synchronized in late G2 phase as described in A. The G2-arrested cells were released or left unreleased, in each case for 20 min in the presence of 10 μM BrdU. DNA was denatured by treatment with HCl for detection of DNA labeled with BrdU. Cells were then double immunostained with anti-LacI and anti-BrdU antibodies, followed by DAPI staining and analysis. **(F)** Representative images of G2-arrested cells or prophase/prometaphase cells with LacI foci. BrdU incorporation (indicating MiDAS) was detected specifically in mitotic cells (yellow arrows), but not in G2 cells (white arrows). Scale bar, 10 μm. **(G)** The graph indicates colocalization frequencies of BrdU foci with LacI foci in G2 phase and prophase/prometaphase cells. Values were calculated from the sum scores of two independent experiments. *, $P < 0.05$; ***, $P < 0.001$; n.s., not significant (χ^2 test). Individual data points from the two independent experiments are also shown.

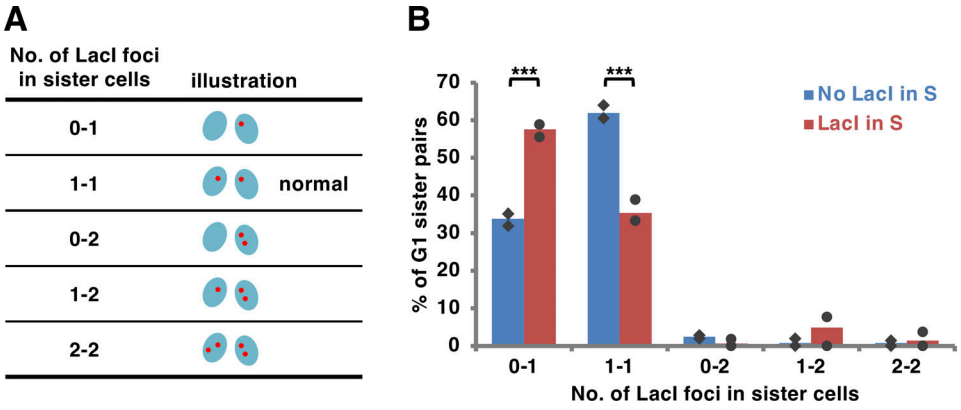

Figure 5. **LacI binding in S phase exacerbates deletion of the *lacO* array in daughter cells. (A and B)** U2OS 40–2-6 ER-LacI cells were synchronized in late G2 phase by treatment with 7 µM RO-3306 for 20 h and 1 µM 4-OHT (for LacI induction) for 20 h or the last 4 h. The G2-arrested cells were then released into fresh medium containing 1 µM 4-OHT for 2 h to enable progression into G1 phase and immunostained with anti-LacI antibody, followed by DAPI staining and analysis. Symmetrical pairs of cells were analyzed as sister cells in G1 phase. **(A)** Depiction of different segregation patterns of LacI foci in sister cells. **(B)** Graph indicating distribution of sister cells with different segregation patterns of LacI foci. Values were calculated from the sum scores of two independent experiments. ***, $P < 0.001$ (χ^2 test). Individual data points from the two independent experiments are also shown.

et al., 2013; Minocherhomji et al., 2015; Duda et al., 2016; Lai et al., 2017; Di Marco et al., 2017), cleavage can also result in deletions from one of the sister chromatids via end joining of the DNA breaks (Naim et al., 2013). As the capacity for MiDAS is limited, it is possible that most underreplicated LacI-bound *lacO* arrays in our model would not be repaired by that pathway. We therefore investigated the influence of S-phase LacI binding on mitotic segregation of the *lacO* array. To monitor the deletion of the *lacO* array, we counted the numbers of LacI foci in paired sister cells defined by symmetrical daughter nuclei in G1 phase (Fig. 5 A). We found that, even in the absence of LacI in S phase, ∼30% of G1-cell pairs contain a *lacO*-deleted sister (Fig. 5 B), which seems to be consistent with our evidence that (post-MiDAS) ∼40% of cells may contain underreplicated *lacO* arrays. Induction of LacI binding in S phase reduced the proportion of cells containing equally segregated *lacO* arrays and increased the frequency of *lacO* deletion (Fig. 5 B). These results suggest that S-phase LacI binding causes *lacO* deletion mediated by the end joining of MUS81-cleaved underreplicated intermediates. As our results have already demonstrated that MUS81 localizes to *lacO* 6–8 h after release from HU arrest (Fig. 2), deletions of the *lacO* arrays might occur during the late-S, G2, and M phases.

Replication stress is known to lead to the generation of ultrafine DNA anaphase bridges (UFBs), which may represent underreplication, at difficult-to-replicate regions (Sarlós et al., 2017; Fragkos and Naim, 2017; Bizard and Hickson, 2018). Therefore, we analyzed mitotic-chromosome abnormalities resulting from replication stress at the *lacO* array. As shown in Fig. 6, A and B, we found that UFB-like DAPI-negative abnormal structures (here referred to as anaphase abnormal *lacO*) are induced by LacI binding in S phase. These structures were located between the two sets of daughter chromosomes and were associated with RPA and PICH (Plk1-interacting checkpoint helicase), a key marker of UFBs (Fig. 6 A; Bizard and Hickson, 2018).

It has been proposed that underreplicated regions are converted to DNA lesions during mitosis, which are shielded by 53BP1 nuclear bodies (NBs) in the daughter cells (Moreno et al., 2016; Lukas et al., 2011; Spies et al., 2019). We examined whether LacI binding induces such 53BP1 NBs by counting the sister cells that contain symmetrical LacI foci associated with 53BP1, and calculating the frequency of such 53BP1-NB-positive cells among the cells in which *lacO* is equally segregated (Fig. 6, C and D). We found that LacI binding in S phase significantly enhances the generation of twin 53BP1-NB–positive cells (Fig. 6 E), indicating that LacI-induced replication stress leads to formation of anaphase abnormal *lacO* structures and DNA lesions that are protected in 53BP1 NBs, through the chromosomal segregation of incomplete replication intermediates.

The ATR pathway ensures sufficient DNA replication before the onset of mitosis, and regulates genome stability (Eykelenboom et al., 2013; Casper et al., 2002). In addition, as we demonstrated above, SLX4 contributes to the accumulation of the DDR factors at the *lacO* sites (Fig. 3 A; and Fig. S4, A and B). We therefore inhibited ATR and SLX4 with VE-821 and siRNA-mediated silencing, respectively, and examined whether the inhibition affects the chromosomal stability of the *lacO* arrays (Fig. 7). The results showed that inhibition of ATR and SLX4 significantly increases the frequency of anaphase abnormal *lacO* structures that are induced by the S-phase LacI binding (Fig. 7), demonstrating that the SLX4–ATR axis contributes to the complete replication and stability of the replication-stressed LacI-bound *lacO* array.

Discussion

Tight DNA–protein interactions impede progression of replication machinery and cause replication stress (Jacome and Fernandez-Capetillo, 2011; Beuzer et al., 2014; Hizume et al., 2018). By taking advantage of the inducible LacI–*lacO* interaction, we have characterized in detail the spatiotemporal regulation of the recruitment of various DDR factors in response to a site-specific replication fork barrier on the human chromosome. DNA replication in S phase enabled accumulation of

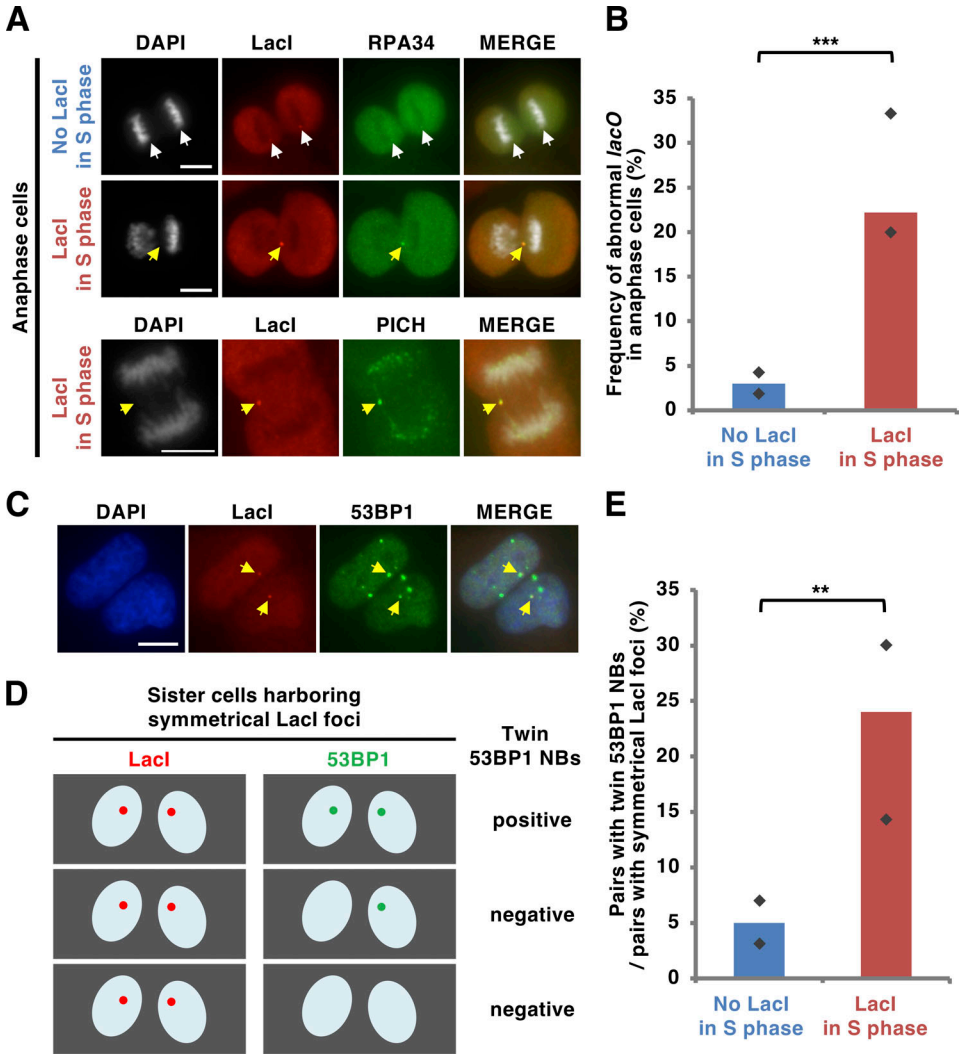

Figure 6. **LacI binding in S phase promotes a UFB-like anaphase abnormal *lacO* array and underreplicated DNA lesions in daughter cells. (A and B)** U2OS 40–2-6 ER-LacI cells were synchronized in late G2 phase by treatment with 7 µM RO-3306 for 20 h and 1 µM 4-OHT (for LacI induction) for 20 h or the last 4 h. The G2-arrested cells were then released into fresh medium for 45 min to enable progression into anaphase and immunostained with the indicated antibodies, followed by DAPI staining and analysis. **(A)** Representative images of anaphase cells. Yellow arrows indicate DAPI-negative anaphase abnormal *lacO* arrays colocalized with RPA and PICH. White arrows denote normally segregated *lacO* arrays. Scale bars, 10 µm. **(B)** The graph indicates frequencies of anaphase abnormal *lacO* per anaphase cell. Values are sum scores from two independent experiments. ***, $P < 0.001$ (χ^2 test). Individual data points from the two independent experiments are also shown. **(C–E)** U2OS 40–2-6 ER-LacI cells were synchronized in late G2 phase and released into G1 phase as described in Fig. 5. Cells were double immunostained with anti-LacI and anti-53BP1 antibodies, followed by DAPI staining and analysis. **(C)** Representative images of twin 53BP1 NBs (indicated by arrows) that colocalize with the symmetrical LacI foci in the sister cells. Scale bar, 10 µm. **(D)** A diagram depicting different patterns of 53BP1 NBs in the sister cells with symmetrical LacI foci. **(E)** The graph indicates frequencies of sister pairs with twin 53BP1 NBs as a percentage of sister pairs harboring symmetrical LacI foci. Values are sum scores from two independent experiments. **, $P < 0.01$ (χ^2 test). Individual data points from the two independent experiments are also shown.

components of the ATR and FA pathways, among which SLX4–XPF functioned as an upstream factor to promote recruitment of DDR proteins, including ATR and FANCD2. S-phase LacI binding caused abnormal mitotic segregation and DNA lesions that remained until the next cell cycle, and the SLX4–ATR axis facilitated complete replication of the LacI-bound *lacO* arrays. Notably, even in the absence of LacI, the *lacO* array was underreplicated, probably because of its nature as a long repetitive sequence, in which it resembles microsatellites, telomeres, and several common fragile sites (Gadaleta and Noguchi, 2017; Kaushal and Freudenreich, 2019; Mirkin and Mirkin, 2007; Tsao and Eckert, 2018). In our ER-LacI induction system, levels of LacI binding to *lacO* sequences in the absence of 4-OHT are ∼25-fold lower than those in the presence of 4-OHT, and the signals are similar extent to those obtained with control IgG (Fig. S2 C). Although we cannot exclude a possibility of very small leaks, we consider that leakiness is not a major reason for the *lacO* instability in the absence of 4-OHT. Our data also clearly showed that LacI binding further exacerbates the replication fork block at the *lacO* array. We also found accumulation of DSB markers 53BP1 and p-ATM in G1 phase. Underreplicated regions can form heritable DNA lesions

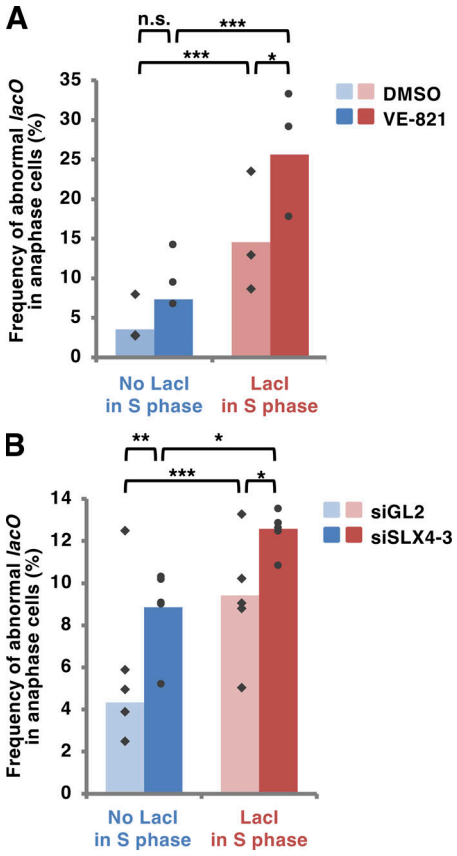

Figure 7. **Inhibition of SLX4-ATR axis increases the frequency of anaphase abnormal *lacO* arrays. (A)** U2OS 40–2-6 ER-LacI cells were synchronized in the late G2 phase by treatment with 7 µM RO-3306 for 20 h and 1 µM 4-OHT (for LacI induction) for 20 h or the last 4 h. During RO-3306 treatment, cells were also treated with 4 µM ATR inhibitor (VE-821) or vehicle only (DMSO) for 20 h. G2-arrested cells were released into fresh medium for 45 min to enable progression into anaphase. The anaphase abnormal *lacO* array was analyzed as described in Fig. 6, A and B. Values are sum scores from three independent experiments. *, P < 0.05; ***, P < 0.001; n.s., not significant (χ^2 test). Individual data points from the three independent experiments are also shown. **(B)** U2OS 40–2-6 ER-LacI cells were transfected with control (siGL2) or SLX4 (siSLX4-3)-targeting siRNAs for 48 h. Cells were then synchronized in the late G2 phase by treatment with 7 µM RO-3306 for 24 h and 1 µM 4-OHT for 24 h or the last 4 h. G2-arrested cells were released into fresh medium for 45 min, followed by analysis as described in A. Values are sum scores from five independent experiments. *, P < 0.05; **, P < 0.01; ***, P < 0.001 (χ^2 test). Individual data points from the five independent experiments are also shown.

that are shielded by 53BP1 in G1 (Spies et al., 2019; Moreno et al., 2016; Lukas et al., 2011), so these results may reflect the persistence of the underreplicated *lacO* array.

Our results suggest that the collision between the DNA replication fork and LacI–*lacO* complex generates an excess of parental-strand ssDNA. LacI–*lacO* interactions have been suggested to inhibit the progression of the CDC45 (cell division cycle 45)–MCM (minichromosome maintenance)–GINS (go-ichi-ni-san) helicase ahead of the polymerase complex (Dewar et al., 2015; Hizume et al., 2018), which is unlikely to cause the accumulation of excess ssDNA at the stalled fork. Instead, unidentified exonucleases may be responsible for nucleolysis of nascent DNA (Pasero and Vindigni, 2017; Liao et al., 2018). Although MRE11 endo/exonuclease has been implicated in the degradation of replication forks stalled by HU (Ray Chaudhuri et al., 2016; Mijic et al., 2017; Schlacher et al., 2011), our results indicate that inhibition of MRE11 does not affect colocalization of RPA with LacI foci (Fig. S4 J), so other exonucleases or helicases may promote the generation of ssDNA at the fork stalled by the DNA–protein complex. For appearance of a small amount of nascent-strand ssDNA, fork reversal could potentially be involved (Pasero and Vindigni, 2017; Liao et al., 2018). We propose that SLX4 and XPF promote DNA cleavage at the stalled fork and trigger generation of ssDNA, probably through the mechanisms discussed above to recruit the effector factors such as ATR and FANCD2, which contribute to genome stability during S phase (Fig. 8). This response seems similar to the fork breakage induced by XPF in the early stage of HU-induced replication stress, which contributes to chromosome stability (Bétous et al., 2018).

FANCD2 has been suggested to function upstream of SLX4 to repair ICL-blocked replication forks (Niraj et al., 2019; Datta and Brosh, 2019; Zhang and Walter, 2014). However, we found that silencing of *FANCD2* results in increased colocalization of SLX4 with LacI foci (Fig. S4 K), possibly in response to an increase in replication fork stress. Branched DNA structures may contribute to the recruitment of SLX4 to LacI-stalled replication forks (Muñoz et al., 2009; Svendsen et al., 2009; Fekairi et al., 2009). We also found that part of SLX4–XPF accumulates on the *lacO* array even in G1-phase or HU-arrested cells (Fig. S3, E and I). It is possible that certain DNA structures and/or DNA lesions derived from underreplication of the *lacO* array may promote the recruitment of SLX4–XPF. Further study is needed to elucidate the mechanisms underlying SLX4–XPF recruitment.

Our results demonstrate that RAD52, but not RAD51, is recruited to LacI foci. The lack of accumulation of RAD51 at the *lacO* site is consistent with previous findings (Luijsterburg et al., 2017). However, RAD51-mediated homology-directed repair pathways have been suggested to operate in response to fork stalling induced by 6×*Ter*–Tus complexes in mouse embryonic stem cells (Willis et al., 2014, 2018). Because our experimental system used much longer repetitive DNA than 6×*Ter*, it is possible that the amount of repeated sequence or DNA–protein complex affects the mechanism underlying the response to replication fork stalling. RAD52 has been implicated both in RAD51-dependent homology-directed repair and RAD51-independent subpathways such as single-strand annealing and break-induced replication–like processes (Bhowmick et al., 2016; Sotiriou et al., 2016; Kramara et al., 2018; Costantino et al., 2014; Verma et al., 2019; Zhang et al., 2019). At the *lacO* array, RAD52 may facilitate annealing of complementary ssDNA to repair the cleaved replication fork. Rebuilding the fork at the same genomic position would be important to preserve the copy number of the repeat sequences. However, it is also possible that RAD52-mediated single-strand annealing at a different genomic position causes chromosomal rearrangement. It will be important in the future to establish the significance of RAD52 for the replication and repeat stability of the *lacO* locus.

Our data demonstrate that FANCD2 and MUS81 accumulate at the *lacO* array in early mitosis, suggesting that, in spite of the activation of the DDR in S phase, a portion of the *lacO* array

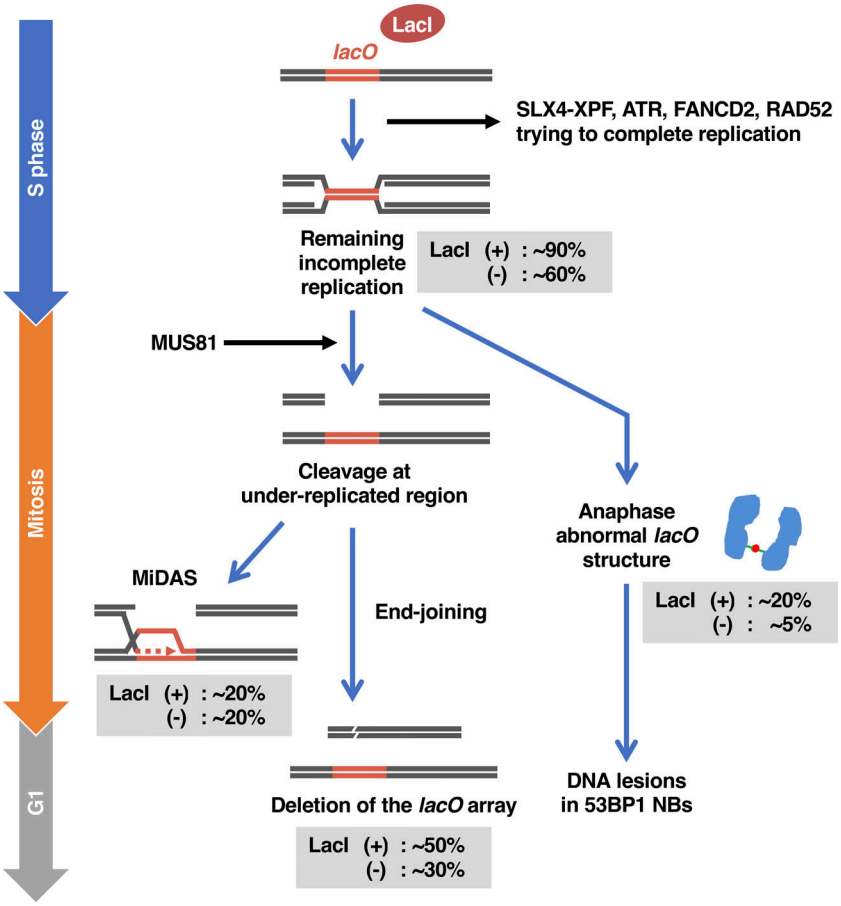

Figure 8. **A model of the fate of underreplicated DNA regions in the *lacO* array.** Even in the absence of LacI binding, the *lacO* array is a difficult-to-replicate region, like other repeat sequences, and contains underreplicated lesions (~60% on the basis of the data shown in Fig. 4 C), which persist until late G2/M phase. Replication stress by LacI binding to the array further increases the frequency of cells with underreplicated DNA lesions (~90%). To try to complete replication of the array during S phase, cells activate the DDR, in which one-ended DSB is first generated by SLX4–XPF–mediated DNA cleavage. Excess ssDNA is then generated by unidentified exonucleases, which in turn recruit ATR, FANCD2, and RAD52. ATR and FANCD2 are interdependently recruited. The DDR may promote completion of replication, because SLX4 and ATR inhibition exacerbates mitotic abnormality induced by LacI. The underreplicated intermediates persisting until late G2/M phase are processed by MUS81-mediated cleavage in early mitosis. Note that cleaved strands are arbitrary in the figure, because it remains unclear whether the cleavage occurs in the leading or lagging strand templates. Cleavage at *lacO* can promote MiDAS (~20% in the absence or presence of LacI; Fig. 4 G) or end joining that results in deletion of the loci (~30% in the absence of LacI and ~50% in the presence of LacI; Fig. 5 B). A fraction of the *lacO* arrays escape from the cleavage and remain underreplicated until anaphase, leading to the anaphase abnormal *lacO* structure (~5% in the absence of LacI and ~20% in the presence of LacI; Fig. 6 B) and the formation of 53BP1 NBs in daughter G1 cells (~5% in the absence of LacI and ~20% in the presence of LacI; Fig. 6 E).

remains underreplicated (Fig. 8). MUS81 associates with SLX4 in a Cdk1-dependent manner and promotes DNA cleavage and subsequent MiDAS at underreplicated regions (Naim et al., 2013; Bhowmick et al., 2016; Duda et al., 2016). Although a small proportion (~20%) of the *lacO* arrays undergo MiDAS, our data also suggest that underreplicated *lacO* arrays that are cleaved by MUS81, but not repaired by MiDAS, may result in deletion of the locus. In addition, some underreplicated *lacO* arrays escape from cleavage and result in anaphase abnormal *lacO* structures. Like single-stranded UFBs, the structures are DAPI negative and coated with RPA and PICH. In addition, a central discrete LacI-positive focus (probably consisting of double-stranded *lacO*) is observed in the structure. It has been suggested that during chromosome segregation, underreplicated dsDNA is converted into ssDNA lesions (Moreno et al., 2016). We therefore speculate that both single-stranded and LacI-bound double-stranded *lacO* derived from underreplicated *lacO* sequences is retained between the separating anaphase chromosomes and observed as the anaphase abnormal structures. For detailed mechanism, further study is needed. On the other hand, Jacome et al. reported that in murine 3T3^{lacO} cells, transfection of LacI (for 48 h) induces a DAPI-positive, PICH-coated anaphase bridge (Jacome and Fernandez-Capetillo, 2011). The difference could be due to difference in the experimental systems such as the difference in time range for LacI induction. Chromosome segregation converts underreplicated regions to DNA lesions, which attract 53BP1 in G1 daughter cells. S-phase LacI binding exacerbates replication stress and increases the frequencies of *lacO* deletion, anaphase abnormality, and 53BP1 NBs. Furthermore, our results support a role for SLX4 and ATR in the completion of replication of LacI-bound *lacO* arrays and prevention of anaphase abnormalities.

In summary, the results of the present study suggest that SLX4–XPF has a key role in generation of excess ssDNA at replication forks arrested by protein–DNA complexes. This mechanism could enable activation of DDR at the blocked replication fork without uncoupling of replicative helicase and polymerase complexes. SLX4–XPF–mediated cleavage may also be a mechanism to resolve topological stress at blocked replication forks. The human genome contains many repetitive elements, which are generally embedded in heterochromatic regions. Unscheduled fork stalling and alteration of repeat length are associated with genomic instability and human disease (Gaillard et al., 2015; Lecona and Fernández-Capetillo, 2014; Padeken et al., 2015). Although further studies are required to determine whether defects in SLX4-dependent DDR signaling are relevant to repeat instability, our findings will provide a novel framework for understanding how such repeat sequences are stably duplicated.

Materials and methods

Cells

U2OS 2-6-3 (Janicki et al., 2004; Higa et al., 2017b) and U2OS 40-2-6 ER-LacI cells were cultured in DMEM supplemented

with 8% FCS. A U2OS 40–2-6 clone overexpressing ER^{T2}-HA-LacI was established as follows. U2OS 2–6-3 cells were cotransfected with pAAVS-CMV-HA-ERT2-LacI (ΔNLS) and AAVS1 T2 CRIPR in pX330 (from Dr. Masato Kanemaki, National Institute of Genetics, Mishima, Japan; Addgene; #72833; Natsume et al., 2016) using Lipofectamine 2000 reagent (Invitrogen), and selected with puromycin (0.5 µg/ml). Expression and 4-OHT-inducible nuclear accumulation of ER^{T2}-HA-LacI protein were confirmed by immunofluorescence analysis (Fig. 1 A). Positive clones were subjected to secondary cloning, and isolated positive clone 40–2-6 was used for further experiments. Cells were cryopreserved in small aliquots and were passaged in the medium for less than 4 mo after resuscitation. We confirmed that the copy number of *lacO* sequences was not significantly changed during cell culture for one month or during siRNA-mediated knockdown of *SLX4* for 48 h (data not shown).

Plasmids

pSV40-HA-LacI has previously been described (Higa et al., 2017b). pET28a-His-T7-LacI was generated by inserting LacI cDNA from pSV40-GFP-LacI (Higa et al., 2017b) into pET28a (Novagen).

To prepare pSV40-HA-ER^{T2}-LacI (ΔNLS), a DNA fragment encoding ER^{T2} was subcloned from pCAG-CreERT2 (from Dr. Connie Cepko, Harvard Medical School, Boston, MA; Addgene #14797; Matsuda and Cepko, 2007) into pSV40-HA-LacI using the In-Fusion HD cloning system (Clontech). The following primers were used: 5′-GATTACGCCCTGTACATATCTGCTGGA GACATGAGAGC-3′ (HA-ER^{T2} forward) and 5′-GGAATTCCTTGT ACAAAGCTGTGGCAGGGAAAC-3′ (ER^{T2}-LacI reverse). Subsequently, pSV40-HA-ER^{T2}-LacI was digested with NotI (New England BioLabs) and Eco81I (Takara Bio), treated with Klenow Fragment (Takara Bio), and self-ligated using the DNA Ligation Kit <Mighty Mix> (Takara Bio) to generate pSV40-HA-ER^{T2}-LacI (ΔNLS).

pAAVS CMV-HA-ER^{T2}-LacI (ΔNLS) was generated by inserting HA-ER^{T2}-LacI (ΔNLS) DNA into pMK231 (AAVS1 CMV-MCS-PURO; from Dr. Masato Kanemaki; Addgene; #105924; Okumura et al., 2018) using the In-Fusion HD cloning system. The following primers were used: 5′-GGACTCAGATCTGCCACC ATGTACCCC-3′ (AAVS1 CMV HA Forward Primer) and 5′-AGC TCGAGATCTTCATCGGGAAACCTGTCG-3′ (LacI rev pMK231 Reverse Primer).

Immunofluorescence staining

To identify colocalization of RPA34, RPA70, ATR, FANCD2, XPF, PICH, and p-ATM with LacI, cells were fixed with 3.7% formaldehyde (Nacalai Tesque) in phosphate-buffered saline (PBS) for 15 min and permeabilized with 0.1% Triton X-100 in PBS for 10 min. For 53BP1, cells were fixed with 3.7% formaldehyde in PBS for 15 min and permeabilized with 0.1% Triton X-100 in mCSK buffer (10 mM Pipes-NaOH, pH 6.8, 100 mM NaCl, 300 mM sucrose, 1 mM EGTA, and 1 mM $MgCl_2$) for 10 min. For SLX1, RAD52, and RAD51, cells were preextracted with 0.1% Triton X-100 in PBS for 10 min before fixation with formaldehyde. For TOPBP1, cells were preextracted with 0.1% Triton X-100 in mCSK buffer for 3 min before fixation with formaldehyde. For MUS81, cells were preextracted with 0.5% Triton X-100 in mCSK buffer for 5 min before fixation with formaldehyde. For staining of SLX4 and BrdU, cells were fixed with chilled 100% methanol for 10 min and then permeabilized with 0.1% Triton X-100 in PBS for 10 min.

After washing with PBS, cells were incubated with appropriate primary antibodies in PBS supplemented with 1% fetal calf serum, followed by incubation with secondary antibodies, and then counterstained with DAPI. Cells were mounted in Fluoro-KEEPER Antifade Reagent (Nacalai Tesque) and analyzed using the BZ-X700 all-in-one fluorescence microscope (Keyence) with CFI Plan Apo λ 40×/0.95 NA objective (Nikon). Microscopic images were acquired by single image captures (5–20 fields for each sample) using the BZ-X viewer software (Keyence). For calculation of colocalization frequencies, at least 60 nuclei with a single prominent LacI focus were scored for each experiment. Frequencies of nuclei in which DDR proteins form a focus on the LacI focus were then manually scored.

Detection of MiDAS

To detect DNA synthesis in mitosis, cells were released from RO-3306–induced G2 synchronization and pulse-labeled with 10 µM BrdU for 20 min. Cells were then fixed and permeabilized simultaneously in PTEMF buffer (20 mM Pipes, pH 6.8, 10 mM EGTA, 0.2% Triton X-100, 1 mM $MgCl_2$, and 4% formaldehyde; Bhowmick et al., 2016) for 20 min. Samples were incubated with rabbit anti-LacI antibody and then with secondary antibody. Subsequently, cells were refixed with 100% methanol for 10 min and then incubated with 1 M HCl for 15 min to denature DNA. Samples were incubated with mouse anti-BrdU antibody (clone 3D4) and then with secondary antibody, followed by counterstaining with DAPI.

ChIP, BrdU immunoprecipitation, and quantitative PCR analysis

ChIP assays were performed as described previously (Higa et al., 2017b). Briefly, cells were fixed with 1% formaldehyde and lysed in SDS lysis buffer (1% SDS, 10 mM EDTA, and 50 mM Tris-HCl, pH 8.0). Chromatin was sonicated into ∼0.5-kb fragments. 5 µg antibodies or control IgG was added to aliquots of each sample, and the samples were incubated for overnight at 4°C. Immunoprecipitates were then collected with 30 µl Dynabeads (Invitrogen). The beads were washed once with RIPA buffer (20 mM Tris-HCl, pH 8.0, 150 mM NaCl, 2 mM EDTA, 1% Triton X-100, and 0.1% SDS), twice with RIPA buffer containing 500 mM NaCl, twice with LiCl wash buffer (10 mM Tris-HCl, pH 8.0, 250 mM LiCl, 1 mM EDTA, 1% NP-40, and 0.5% sodium deoxycholate), and once with Tris-EDTA buffer (10 mM Tris, pH 8.0, and 1 mM EDTA). The immunocomplexes were eluted with ChIP elution buffer (100 mM $NaHCO_3$ and 1% SDS) at RT for 15 min. After cross-linking reversal, phenol/chloroform extraction, and ethanol precipitation, DNA was dissolved in Tris-EDTA buffer.

BrdU immunoprecipitation assays were performed as described previously, with some modifications (Verma et al., 2018). Briefly, U2OS 40–2-6 ER-LacI cells were treated with 1 µM 4-OHT for 80 min. Cells were labeled with BrdU for the last 20 min. Genomic DNA was purified and sonicated to give

~0.5-kb fragments. Anti-BrdU antibody (clone B44, 3 µg) was added to an aliquot of genomic DNA (4 µg) and incubated overnight at 4°C. Immunoprecipitates were collected with 20 µl Dynabeads. The beads were washed three times with 0.0625% Triton X-100 in PBS, and once with Tris-EDTA buffer. The immunocomplexes were eluted with ChIP elution buffer at RT for 15 min. After phenol/chloroform extraction and ethanol precipitation, DNA was dissolved in Tris-EDTA buffer.

PCR reactions were performed as described previously (Sugimoto et al., 2011; Higa et al., 2017b) using the iCycler iQ real-time PCR detection system (Bio-Rad) or the CFX96 Touch system (Bio-Rad). TB Green Premix Ex Taq II (Takara Bio) was used according to the manufacturer's instructions. The following primers were used to detect the *lacO* sequence: 5′-TAGAGG CGCCGAATTGCACA-3′ and 5′-GCCACAAATTGTTATCCGCTCA-3′. The cycling parameters were as follows: 1 min at 95°C and then 50 cycles at 95°C for 30 s, at 64.2°C for 30 s, and at 72°C for 30 s. For the *LMNB2* origin, following primers were used: 5′-GGC TGGCATGGACTTTCATTTCAG-3′ and 5′-GTGGAGGGATCTTTC TTAGACATC-3′. The cycling parameters were as follows: 1 min at 95°C; five cycles at 95°C for 30 s, 66.9°C for 30 s, and 72°C for 30 s; five cycles at 95°C for 30 s, 64.9°C for 30 s, and 72°C for 30 s; and 50 cycles at 95°C for 30 s, 62.9°C for 30 s, and 72°C for 30 s.

Drugs

The following drugs were used: 4-OHT (Abcam), RO-3306 (Sigma), HU (Sigma), lovastatin (LKT Laboratories), VE-821 (Haoyuan Chemexpress), KU-55933 (Sigma), and mirin (Sigma).

Cell synchronization

For G1-phase synchronization, cells were synchronized with 40 µM lovastatin for 40 h and analyzed. For S-phase synchronization, cells were synchronized with 2.5 mM HU for 18 h and released into fresh medium. For the experiment shown in Fig. 1 E, at 4 h after release from HU, cells were further treated with 1 µM 4-OHT for 2 h and then analyzed. For G2/M-phase synchronization, cells were synchronized in the late G2 phase by incubation with 7 µM RO-3306 for 20 h (Figs. 4, 5, 6, and 7 A) or 24 h (Fig. 7 B) and then released into fresh medium.

Cell-cycle analysis

Cell-cycle analysis was performed essentially as described previously (Yokoyama et al., 2019; Sugimoto et al., 2011). For the experiments shown in Fig. S3, A and F, cells were treated with a CycleTEST PLUS DNA reagent kit (Becton Dickinson). For the experiments shown in Fig. 4 B and Fig. S3 C, cells were suspended in PBS containing 0.1% TritonX-100 and RNase (10 µg/ml) and then stained with propidium iodide (40 µg/ml). Cells were then analyzed with a FACSCalibur flow cytometer (BD Bioscience).

siRNA experiments

U2OS 40-2-6 ER-LacI cells were transfected with 12 nM siRNA duplexes using Lipofectamine RNAiMAX (Invitrogen) according to the manufacturer's instructions. siRNA oligonucleotides with the following sequences (sense strand) were synthesized (IDT or Dharmacon): siGL2 (5′-CGUACGCGGAAUACUUCGAdTdT-3′), siGFP (5′-ACCCUGAAGUUCAUCUGCACCACdCdG-3′), siLuci (5′-GGUUCCUGGAACAAUUGCUUUUAdCdA-3′), siSLX4-3 (5′-AAACGUGAAUGAAGCAGAAUU-3′; Duda et al., 2016), siSLX4-4 (5′-CGGCAUUUGAGUCUGCAGGUGUU-3′; Duda et al., 2016), siXPF1-1 (5′-CUUUUCUAAAAGCUAGAUCAGCAdTdT-3′), siXPF1-2 (5′-CUUGACUGAUAGAAUACCUUCAGdAdT-3′), siMUS81-1 (5′-GGGGCAUUGCAGCUUGGAAUCUAdTdT-3′), siMUS81-2 (5′-AGAG-CAUGGUUCCGUCCACAACCdTdC-3′), siFANCD2-1 (5′-GAUGUU-CUGAGCUUACUGGAAACdCdT-3′), and siFANCD2-2 (5′-GGA UUUACCUGUGAUAAUAAAGUdTdC-3′).

Antibodies

Rabbit anti-LacI antibody was obtained by immunizing rabbits with a bacterially produced His-T7-LacI protein. Mouse antibodies against human RPA34 and RPA70 were provided by Dr. Murakami (Hokkaido University, Sapporo, Japan).

Other antibodies used in this study were as follows: ATR (Santa Cruz; Goat, sc1887), ATRIP (Cell Signaling; Rabbit, #2737), RPA34 (Calbiochem; Mouse, NA19L), TOPBP1 (Abcam; Rabbit, ab2402), FANCD2 (Novus; Rabbit, NB100-182), LacI (clone 9A5, Merck, Mouse, #05-503), HA (clone 3F10; Roche; Rat, 11867423001), Chk1 (Santa Cruz; Mouse, sc-8408), phosphorylated Chk1 (Ser345; Cell Signaling; Rabbit, #2348S), phosphorylated ATM (Ser1981; Rockland; Mouse, 200–301-400; Abcam; Rabbit, ab81292), 53BP1 (Novus; Rabbit, NB100-904), RAD51 (BioAcademia; Rabbit, 70–012), RAD52 (BioAcademia; Rabbit, 70–015), BrdU (clone 3D4 and B44; BD PharMingen; Mouse, 555627 and 347580, respectively), Cyclin A (Santa Cruz; Rabbit, sc-596), Cyclin E (Santa Cruz; Mouse, sc-247), SLX4 (Novus; Rabbit, NBP1-28680), XPF (Bethyl; Rabbit, A301-315A), MUS81 (Abcam; Mouse, ab14387), SLX1 (Atlas Antibodies; Rabbit, HPA047038), PICH (clone 142–26-3, Merck, Mouse, 04–1540), goat normal IgG (Chemicon; PP40), mouse normal IgG (Southern Biotech; 0107–01), and rabbit normal IgG (Dako; X0903).

Specificity of the immunofluorescence signal derived from the anti-SLX1 antibody we used was confirmed by the finding that the siRNA-mediated knockdown significantly reduces the accumulation of SLX1 at the *lacO* array (data not shown). However, this antibody was not applicable to detect SLX1 protein in our immunoblotting experiments.

The following secondary antibodies were used: HRP-conjugated rabbit anti-mouse IgG (H + L; Invitrogen; 61–6520), HRP-conjugated goat anti-rabbit IgG (H + L; Invitrogen; 65–6120), Alexa488-conjugated goat anti-rabbit IgG (Invitrogen; A11034), Alexa488-conjugated goat anti-mouse IgG (Invitrogen; A11029 and A11001); Alexa594-conjugated donkey anti-rabbit IgG (Invitrogen; A21207), CF488A-conjugated goat anti-rabbit IgG (Biotium; 20019), CF488A-conjugated donkey anti-goat IgG (Biotium; 20016), CF594-conjugated donkey anti-rat IgG (Biotium; 20159), and CF594 goat anti-mouse IgG (Biotium; 20111).

Immunoblotting

Immunoblotting was performed as previously described (Fujiyama et al., 2020). Antibody binding was visualized with HRP-conjugated secondary antibodies using EzWestLumi One (ATTO) or Chemi-Lumi One Super (Nacalai Tesque). Chemiluminescent signals were captured via a cooled-CCD (charge-coupled device) camera direct detection system (Aisin; LumiVision Imager).

Data presentation and statistical analysis

Unless otherwise stated, quantitative data are represented as the mean ± SD of three or more independent experiments. For Fig. 1, D and E; Fig. 3, C–E; Fig. 4, C, D, and G; Fig. 5 B; Fig. 6, B and E; Fig. S3, E and I; and Fig. S4, B, D, F, H, J, and K; data were calculated from the sum scores of two independent experiments. As described in the figures, statistical significance was assessed by using an unpaired two-tailed Student's *t* test or a χ^2 test. P values < 0.05 were considered statistically significant. For the *t* tests, data distribution was assumed to be normal but this was not formally tested. For qualitative data and semiquantitative data, a representative image from multiple independent experiments is shown; for all such figures, essentially the same results were obtained in the multiple independent experiments.

Online supplemental material

Fig. S1 shows the recruitment of DDR proteins to *lacO* arrays and the activation of DDR after transient expression of HA-LacI in U2OS 2-6-3 cells. Fig. S2 shows the recruitment of DDR proteins to *lacO* arrays in U2OS 40-2-6 ER-LacI cells. Fig. S3 shows cell-cycle profiles of U2OS 40-2-6 ER-LacI cells and additional experiments to investigate the effect of cell-cycle synchronization. Fig. S4 shows additional data for silencing of *SLX4*, *XPF*, *MUS81*, and *FANCD2*, and the SLX4–XPF-dependent accumulation of DDR factors.

Acknowledgments

We thank Dr. Masato Kanemaki (National Institute of Genetics, Mishima, Japan) for plasmids and Dr. Yota Murakami (Hokkaido University, Sapporo, Japan) for antibodies. We appreciate the technical support received from the Research Support Center, Research Center for Human Disease Modeling, Kyushu University Graduate School of Medical Sciences.

This investigation was supported in part by the Japan Society for the Promotion of Science (KAKENHI grant JP15K18478 to K. Yoshida). K. Yoshida is also supported by research grants from the Fukuoka Foundation for Sound Health Cancer Research Fund and the Mochida Memorial Foundation for Medical and Pharmaceutical Research.

The authors declare no competing financial interests.

Author contributions: K. Yoshida and M. Fujita designed and managed the project. R. Ishimoto, Y. Tsuzuki, T. Matsumura, S. Kurashige, K. Enokitani, K. Narimatsu, M. Higa, and K. Yoshida conducted the experiments and data analysis. N. Sugimoto and M. Fujita supervised the experiments and data analysis. R. Ishimoto, K. Yoshida, and M. Fujita wrote the manuscript.

Submitted: 23 March 2020
Revised: 5 October 2020
Accepted: 13 November 2020

References

Ait Saada, A., S.A.E. Lambert, and A.M. Carr. 2018. Preserving replication fork integrity and competence via the homologous recombination pathway. *DNA Repair (Amst.)*. 71:135–147. https://doi.org/10.1016/j.dnarep.2018.08.017

Anantha, R.W., V.M. Vassin, and J.A. Borowiec. 2007. Sequential and synergistic modification of human RPA stimulates chromosomal DNA repair. *J. Biol. Chem.* 282:35910–35923. https://doi.org/10.1074/jbc.M704645200

Bétous, R., T. Goullet de Rugy, A.L. Pelegrini, S. Queille, J.P. de Villartay, and J.S. Hoffmann. 2018. DNA replication stress triggers rapid DNA replication fork breakage by Artemis and XPF. *PLoS Genet.* 14:e1007541. https://doi.org/10.1371/journal.pgen.1007541

Beuzer, P., J.P. Quivy, and G. Almouzni. 2014. Establishment of a replication fork barrier following induction of DNA binding in mammalian cells. *Cell Cycle.* 13:1607–1616. https://doi.org/10.4161/cc.28627

Bhowmick, R., S. Minocherhomji, and I.D. Hickson. 2016. RAD52 Facilitates Mitotic DNA Synthesis Following Replication Stress. *Mol. Cell.* 64:1117–1126. https://doi.org/10.1016/j.molcel.2016.10.037

Bizard, A.H., and I.D. Hickson. 2018. Anaphase: a fortune-teller of genomic instability. *Curr. Opin. Cell Biol.* 52:112–119. https://doi.org/10.1016/j.ceb.2018.02.012

Black, E.M., and S. Giunta. 2018. Repetitive fragile sites: Centromere satellite DNA as a source of genome instability in human diseases. *Genes (Basel).* 9:615. https://doi.org/10.3390/genes9120615

Blackford, A.N., and S.P. Jackson. 2017. ATM, ATR, and DNA-PK: The Trinity at the Heart of the DNA Damage Response. *Mol. Cell.* 66:801–817. https://doi.org/10.1016/j.molcel.2017.05.015

Buisson, R., J.L. Boisvert, C.H. Benes, and L. Zou. 2015. Distinct but Concerted Roles of ATR, DNA-PK, and Chk1 in Countering Replication Stress during S Phase. *Mol. Cell.* 59:1011–1024. https://doi.org/10.1016/j.molcel.2015.07.029

Casper, A.M., P. Nghiem, M.F. Arlt, and T.W. Glover. 2002. ATR regulates fragile site stability. *Cell.* 111:779–789. https://doi.org/10.1016/S0092-8674(02)01113-3

Chan, K.L., T. Palmai-Pallag, S. Ying, and I.D. Hickson. 2009. Replication stress induces sister-chromatid bridging at fragile site loci in mitosis. *Nat. Cell Biol.* 11:753–760. https://doi.org/10.1038/ncb1882

Costantino, L., S.K. Sotiriou, J.K. Rantala, S. Magin, E. Mladenov, T. Helleday, J.E. Haber, G. Iliakis, O.P. Kallioniemi, and T.D. Halazonetis. 2014. Break-induced replication repair of damaged forks induces genomic duplications in human cells. *Science.* 343:88–91. https://doi.org/10.1126/science.1243211

Couch, F.B., C.E. Bansbach, R. Driscoll, J.W. Luzwick, G.G. Glick, R. Bétous, C.M. Carroll, S.Y. Jung, J. Qin, K.A. Cimprich, and D. Cortez. 2013. ATR phosphorylates SMARCAL1 to prevent replication fork collapse. *Genes Dev.* 27:1610–1623. https://doi.org/10.1101/gad.214080.113

Dalgaard, J.Z., E.L. Godfrey, and R.J. MacFarlane. 2011. Eukaryotic Replication Barriers: How, Why and Where Forks Stall. *In* DNA Replication-Current Advances. H. Seligmann, editor. InTech. 269–304.

Datta, A., and R.M. Brosh Jr. 2019. Holding all the cards—how fanconi anemia proteins deal with replication stress and preserve genomic stability. *Genes (Basel).* 10:170. https://doi.org/10.3390/genes10020170

Debatisse, M., and F. Rosselli. 2019. A journey with common fragile sites: From S phase to telophase. *Genes Chromosomes Cancer.* 58:305–316. https://doi.org/10.1002/gcc.22704

Dehé, P.M., and P.H.L. Gaillard. 2017. Control of structure-specific endonucleases to maintain genome stability. *Nat. Rev. Mol. Cell Biol.* 18:315–330. https://doi.org/10.1038/nrm.2016.177

Dewar, J.M., M. Budzowska, and J.C. Walter. 2015. The mechanism of DNA replication termination in vertebrates. *Nature.* 525:345–350. https://doi.org/10.1038/nature14887

Di Marco, S., Z. Hasanova, R. Kanagaraj, N. Chappidi, V. Altmannova, S. Menon, H. Sedlackova, J. Langhoff, K. Surendranath, D. Hühn, et al. 2017. RECQ5 Helicase Cooperates with MUS81 Endonuclease in Processing Stalled Replication Forks at Common Fragile Sites during Mitosis. *Mol. Cell.* 66:658–671.e8. https://doi.org/10.1016/j.molcel.2017.05.006

Duda, H., M. Arter, J. Gloggnitzer, F. Teloni, P. Wild, M.G. Blanco, M. Altmeyer, and J. Matos. 2016. A Mechanism for Controlled Breakage of Under-replicated Chromosomes during Mitosis. *Dev. Cell.* 39:740–755. https://doi.org/10.1016/j.devcel.2016.11.017

Eykelenboom, J.K., E.C. Harte, L. Canavan, A. Pastor-Peidro, I. Calvo-Asensio, M. Llorens-Agost, and N.F. Lowndes. 2013. ATR activates the S-M checkpoint during unperturbed growth to ensure sufficient replication prior to mitotic onset. *Cell Rep.* 5:1095–1107. https://doi.org/10.1016/j.celrep.2013.10.027

Fekairi, S., S. Scaglione, C. Chahwan, E.R. Taylor, A. Tissier, S. Coulon, M.Q. Dong, C. Ruse, J.R. Yates III, P. Russell, et al. 2009. Human SLX4 is a Holliday junction resolvase subunit that binds multiple DNA repair/recombination endonucleases. *Cell.* 138:78–89. https://doi.org/10.1016/j.cell.2009.06.029

Fragkos, M., and V. Naim. 2017. Rescue from replication stress during mitosis. *Cell Cycle*. 16:613–633. https://doi.org/10.1080/15384101.2017.1288322

Fujiyama, H., T. Tsuji, K. Hironaka, K. Yoshida, N. Sugimoto, and M. Fujita. 2020. GRWD1 directly interacts with p53 and negatively regulates p53 transcriptional activity. *J. Biochem.* 167:15–24. https://doi.org/10.1093/jb/mvz075

Gadaleta, M.C., and E. Noguchi. 2017. Regulation of DNA replication through natural impediments in the eukaryotic genome. *Genes (Basel)*. 8:98. https://doi.org/10.3390/genes8030098

Gaillard, H., T. García-Muse, and A. Aguilera. 2015. Replication stress and cancer. *Nat. Rev. Cancer*. 15:276–289. https://doi.org/10.1038/nrc3916

García-Muse, T., and A. Aguilera. 2016. Transcription-replication conflicts: how they occur and how they are resolved. *Nat. Rev. Mol. Cell Biol.* 17:553–563. https://doi.org/10.1038/nrm.2016.88

Helleday, T. 2003. Pathways for mitotic homologous recombination in mammalian cells. *Mutat. Res.* 532:103–115. https://doi.org/10.1016/j.mrfmmm.2003.08.013

Higa, M., M. Fujita, and K. Yoshida. 2017a. DNA replication origins and fork progression at mammalian telomeres. *Genes (Basel)*. 8:112. https://doi.org/10.3390/genes8040112

Higa, M., T. Kushiyama, S. Kurashige, D. Kohmon, K. Enokitani, S. Iwahori, N. Sugimoto, K. Yoshida, and M. Fujita. 2017b. TRF2 recruits ORC through TRFH domain dimerization. *Biochim. Biophys. Acta Mol. Cell Res.* 1864:191–201. https://doi.org/10.1016/j.bbamcr.2016.11.004

Hills, S.A., and J.F.X. Diffley. 2014. DNA replication and oncogene-induced replicative stress. *Curr. Biol.* 24:R435–R444. https://doi.org/10.1016/j.cub.2014.04.012

Hizume, K., S. Endo, S. Muramatsu, T. Kobayashi, and H. Araki. 2018. DNA polymerase ε-dependent modulation of the pausing property of the CMG helicase at the barrier. *Genes Dev.* 32:1315–1320. https://doi.org/10.1101/gad.317073.118

Ishiai, M., K. Sato, J. Tomida, H. Kitao, H. Kurumizaka, and M. Takata. 2017. Activation of the FA pathway mediated by phosphorylation and ubiquitination. *Mutat. Res.* 803-805:89–95. https://doi.org/10.1016/j.mrfmmm.2017.05.003

Jacome, A., and O. Fernandez-Capetillo. 2011. Lac operator repeats generate a traceable fragile site in mammalian cells. *EMBO Rep.* 12:1032–1038. https://doi.org/10.1038/embor.2011.158

Janicki, S.M., T. Tsukamoto, S.E. Salghetti, W.P. Tansey, R. Sachidanandam, K.V. Prasanth, T. Ried, Y. Shav-Tal, E. Bertrand, R.H. Singer, and D.L. Spector. 2004. From silencing to gene expression: real-time analysis in single cells. *Cell*. 116:683–698. https://doi.org/10.1016/S0092-8674(04)00171-0

Kaushal, S., and C.H. Freudenreich. 2019. The role of fork stalling and DNA structures in causing chromosome fragility. *Genes Chromosomes Cancer*. 58:270–283. https://doi.org/10.1002/gcc.22721

Kim, S.M., and S.L. Forsburg. 2018. Regulation of structure-specific endonucleases in replication stress. *Genes (Basel)*. 9:634. https://doi.org/10.3390/genes9120634

Kim, J., D. Sturgill, R. Sebastian, S. Khurana, A.D. Tran, G.B. Edwards, A. Kruswick, S. Burkett, E.K. Hosogane, W.W. Hannon, et al. 2018. Replication Stress Shapes a Protective Chromatin Environment across Fragile Genomic Regions. *Mol. Cell.* 69:36–47.e7. https://doi.org/10.1016/j.molcel.2017.11.021

Kotsantis, P., E. Petermann, and S.J. Boulton. 2018. Mechanisms of oncogene-induced replication stress: Jigsaw falling into place. *Cancer Discov.* 8:537–555. https://doi.org/10.1158/2159-8290.CD-17-1461

Kramara, J., B. Osia, and A. Malkova. 2018. Break-Induced Replication: The Where, The Why, and The How. *Trends Genet.* 34:518–531. https://doi.org/10.1016/j.tig.2018.04.002

Lai, X., R. Broderick, V. Bergoglio, J. Zimmer, S. Badie, W. Niedzwiedz, J.S. Hoffmann, and M. Tarsounas. 2017. MUS81 nuclease activity is essential for replication stress tolerance and chromosome segregation in BRCA2-deficient cells. *Nat. Commun.* 8:15983. https://doi.org/10.1038/ncomms15983

Lambert, S., and A.M. Carr. 2013. Impediments to replication fork movement: stabilisation, reactivation and genome instability. *Chromosoma*. 122:33–45. https://doi.org/10.1007/s00412-013-0398-9

Lecona, E., and O. Fernández-Capetillo. 2014. Replication stress and cancer: it takes two to tango. *Exp. Cell Res.* 329:26–34. https://doi.org/10.1016/j.yexcr.2014.09.019

Liao, H., F. Ji, T. Helleday, and S. Ying. 2018. Mechanisms for stalled replication fork stabilization: new targets for synthetic lethality strategies in cancer treatments. *EMBO Rep.* 19:e46263. https://doi.org/10.15252/embr.201846263

Luijsterburg, M.S., D. Typas, M.C. Caron, W.W. Wiegant, D. van den Heuvel, R.A. Boonen, A.M. Couturier, L.H. Mullenders, J.Y. Masson, and H. van Attikum. 2017. A PALB2-interacting domain in RNF168 couples homologous recombination to DNA break-induced chromatin ubiquitylation. *eLife*. 6:e20922. https://doi.org/10.7554/eLife.20922

Lukas, C., V. Savic, S. Bekker-Jensen, C. Doil, B. Neumann, R.S. Pedersen, M. Grøfte, K.L. Chan, I.D. Hickson, J. Bartek, and J. Lukas. 2011. 53BP1 nuclear bodies form around DNA lesions generated by mitotic transmission of chromosomes under replication stress. *Nat. Cell Biol.* 13:243–253. https://doi.org/10.1038/ncb2201

Magdalou, I., B.S. Lopez, P. Pasero, and S.A.E. Lambert. 2014. The causes of replication stress and their consequences on genome stability and cell fate. *Semin. Cell Dev. Biol.* 30:154–164. https://doi.org/10.1016/j.semcdb.2014.04.035

Matsuda, T., and C.L. Cepko. 2007. Controlled expression of transgenes introduced by in vivo electroporation. *Proc. Natl. Acad. Sci. USA*. 104:1027–1032. https://doi.org/10.1073/pnas.0610155104

Michl, J., J. Zimmer, and M. Tarsounas. 2016. Interplay between Fanconi anemia and homologous recombination pathways in genome integrity. *EMBO J.* 35:909–923. https://doi.org/10.15252/embj.201693860

Mijic, S., R. Zellweger, N. Chappidi, M. Berti, K. Jacobs, K. Mutreja, S. Ursich, A. Ray Chaudhuri, A. Nussenzweig, P. Janscak, and M. Lopes. 2017. Replication fork reversal triggers fork degradation in BRCA2-defective cells. *Nat. Commun.* 8:859. https://doi.org/10.1038/s41467-017-01164-5

Minocherhomji, S., and I.D. Hickson. 2014. Structure-specific endonucleases: guardians of fragile site stability. *Trends Cell Biol.* 24:321–327. https://doi.org/10.1016/j.tcb.2013.11.007

Minocherhomji, S., S. Ying, V.A. Bjerregaard, S. Bursomanno, A. Aleliunaite, W. Wu, H.W. Mankouri, H. Shen, Y. Liu, and I.D. Hickson. 2015. Replication stress activates DNA repair synthesis in mitosis. *Nature*. 528:286–290. https://doi.org/10.1038/nature16139

Mirkin, E.V., and S.M. Mirkin. 2007. Replication fork stalling at natural impediments. *Microbiol. Mol. Biol. Rev.* 71:13–35. https://doi.org/10.1128/MMBR.00030-06

Mladenov, E., S. Magin, A. Soni, and G. Iliakis. 2016. DNA double-strand-break repair in higher eukaryotes and its role in genomic instability and cancer: Cell cycle and proliferation-dependent regulation. *Semin. Cancer Biol.* 37-38:51–64. https://doi.org/10.1016/j.semcancer.2016.03.003

Moreno, A., J.T. Carrington, L. Albergante, M. Al Mamun, E.J. Haagensen, E.S. Komseli, V.G. Gorgoulis, T.J. Newman, and J.J. Blow. 2016. Unreplicated DNA remaining from unperturbed S phases passes through mitosis for resolution in daughter cells. *Proc. Natl. Acad. Sci. USA*. 113:E5757–E5764. https://doi.org/10.1073/pnas.1603252113

Muñoz, S., and J. Méndez. 2017. DNA replication stress: from molecular mechanisms to human disease. *Chromosoma*. 126:1–15. https://doi.org/10.1007/s00412-016-0573-x

Muñoz, I.M., K. Hain, A.C. Déclais, M. Gardiner, G.W. Toh, L. Sanchez-Pulido, J.M. Heuckmann, R. Toth, T. Macartney, B. Eppink, et al. 2009. Coordination of structure-specific nucleases by human SLX4/BTBD12 is required for DNA repair. *Mol. Cell.* 35:116–127. https://doi.org/10.1016/j.molcel.2009.06.020

Naim, V., T. Wilhelm, M. Debatisse, and F. Rosselli. 2013. ERCC1 and MUS81-EME1 promote sister chromatid separation by processing late replication intermediates at common fragile sites during mitosis. *Nat. Cell Biol.* 15:1008–1015. https://doi.org/10.1038/ncb2793

Natsume, T., T. Kiyomitsu, Y. Saga, and M.T. Kanemaki. 2016. Rapid Protein Depletion in Human Cells by Auxin-Inducible Degron Tagging with Short Homology Donors. *Cell Rep.* 15:210–218. https://doi.org/10.1016/j.celrep.2016.03.001

Nickoloff, J.A., D. Jones, S.H. Lee, E.A. Williamson, and R. Hromas. 2017. Drugging the Cancers Addicted to DNA Repair. *J. Natl. Cancer Inst.* 109:djx059. https://doi.org/10.1093/jnci/djx059

Niraj, J., A. Färkkilä, and A.D. D'Andrea. 2019. The Fanconi Anemia Pathway in Cancer. *Annu. Rev. Cancer Biol.* 3:457–478. https://doi.org/10.1146/annurev-cancerbio-030617-050422

Okumura, M., T. Natsume, M.T. Kanemaki, and T. Kiyomitsu. 2018. Dynein-Dynactin-NuMA clusters generate cortical spindle-pulling forces as a multi-arm ensemble. *eLife*. 7:e36559. https://doi.org/10.7554/eLife.36559

Özer, Ö., and I.D. Hickson. 2018. Pathways for maintenance of telomeres and common fragile sites during DNA replication stress. *Open Biol.* 8:180018. https://doi.org/10.1098/rsob.180018

Padeken, J., P. Zeller, and S.M. Gasser. 2015. Repeat DNA in genome organization and stability. *Curr. Opin. Genet. Dev.* 31:12–19. https://doi.org/10.1016/j.gde.2015.03.009

Panier, S., M. Maric, G. Hewitt, E. Mason-Osann, H. Gali, A. Dai, A. Labadorf, J.H. Guervilly, P. Ruis, S. Segura-Bayona, et al. 2019. SLX4IP Antagonizes Promiscuous BLM Activity during ALT Maintenance. *Mol. Cell.* 76: 27–43.e11. https://doi.org/10.1016/j.molcel.2019.07.010

Pasero, P., and A. Vindigni. 2017. Nucleases Acting at Stalled Forks: How to Reboot the Replication Program with a Few Shortcuts. *Annu. Rev. Genet.* 51:477–499. https://doi.org/10.1146/annurev-genet-120116-024745

Ray Chaudhuri, A., E. Callen, X. Ding, E. Gogola, A.A. Duarte, J.E. Lee, N. Wong, V. Lafarga, J.A. Calvo, N.J. Panzarino, et al. 2016. Replication fork stability confers chemoresistance in BRCA-deficient cells. *Nature.* 535: 382–387. https://doi.org/10.1038/nature18325

Saldivar, J.C., D. Cortez, and K.A. Cimprich. 2017. The essential kinase ATR: ensuring faithful duplication of a challenging genome. *Nat. Rev. Mol. Cell Biol.* 18:622–636. https://doi.org/10.1038/nrm.2017.67

Salim, D., and J.L. Gerton. 2019. Ribosomal DNA instability and genome adaptability. *Chromosome Res.* 27:73–87. https://doi.org/10.1007/s10577-018-9599-7

Sarbajna, S., D. Davies, and S.C. West. 2014. Roles of SLX1-SLX4, MUS81-EME1, and GEN1 in avoiding genome instability and mitotic catastrophe. *Genes Dev.* 28:1124–1136. https://doi.org/10.1101/gad.238303.114

Sarlós, K., A. Biebricher, E.J.G. Petermann, G.J.L. Wuite, and I.D. Hickson. 2017. Knotty Problems during Mitosis: Mechanistic Insight into the Processing of Ultrafine DNA Bridges in Anaphase. *Cold Spring Harb. Symp. Quant. Biol.* 82:187–195. https://doi.org/10.1101/sqb.2017.82.033647

Schlacher, K., N. Christ, N. Siaud, A. Egashira, H. Wu, and M. Jasin. 2011. Double-strand break repair-independent role for BRCA2 in blocking stalled replication fork degradation by MRE11. *Cell.* 145:529–542. https://doi.org/10.1016/j.cell.2011.03.041

Sotiriou, S.K., I. Kamileri, N. Lugli, K. Evangelou, C. Da-Ré, F. Huber, L. Padayachy, S. Tardy, N.L. Nicati, S. Barriot, et al. 2016. Mammalian RAD52 Functions in Break-Induced Replication Repair of Collapsed DNA Replication Forks. *Mol. Cell.* 64:1127–1134. https://doi.org/10.1016/j.molcel.2016.10.038

Spies, J., C. Lukas, K. Somyajit, M.B. Rask, J. Lukas, and K.J. Neelsen. 2019. 53BP1 nuclear bodies enforce replication timing at under-replicated DNA to limit heritable DNA damage. *Nat. Cell Biol.* 21:487–497. https://doi.org/10.1038/s41556-019-0293-6

Sugimoto, N., T. Yugawa, M. Iizuka, T. Kiyono, and M. Fujita. 2011. Chromatin remodeler sucrose nonfermenting 2 homolog (SNF2H) is recruited onto DNA replication origins through interaction with Cdc10 protein-dependent transcript 1 (Cdt1) and promotes pre-replication complex formation. *J. Biol. Chem.* 286:39200–39210. https://doi.org/10.1074/jbc.M111.256123

Svendsen, J.M., A. Smogorzewska, M.E. Sowa, B.C. O'Connell, S.P. Gygi, S.J. Elledge, and J.W. Harper. 2009. Mammalian BTBD12/SLX4 assembles a Holliday junction resolvase and is required for DNA repair. *Cell.* 138: 63–77. https://doi.org/10.1016/j.cell.2009.06.030

Syeda, A.H., M. Hawkins, and P. McGlynn. 2014. Recombination and replication. *Cold Spring Harb. Perspect. Biol.* 6:a016550. https://doi.org/10.1101/cshperspect.a016550

Toledo, L., K.J. Neelsen, and J. Lukas. 2017. Replication Catastrophe: When a Checkpoint Fails because of Exhaustion. *Mol. Cell.* 66:735–749. https://doi.org/10.1016/j.molcel.2017.05.001

Tsao, W.C., and K.A. Eckert. 2018. Detours to replication: Functions of specialized DNA polymerases during oncogene-induced replication stress. *Int. J. Mol. Sci.* 19:3255. https://doi.org/10.3390/ijms19103255

Verma, P., R.L. Dilley, M.T. Gyparaki, and R.A. Greenberg. 2018. Direct Quantitative Monitoring of Homology-Directed DNA Repair of Damaged Telomeres. *In* Methods in Enzymology. Elsevier Inc. 107–134.

Verma, P., R.L. Dilley, T. Zhang, M.T. Gyparaki, Y. Li, and R.A. Greenberg. 2019. RAD52 and SLX4 act nonepistatically to ensure telomere stability during alternative telomere lengthening. *Genes Dev.* 33:221–235. https://doi.org/10.1101/gad.319723.118

Willis, N.A., G. Chandramouly, B. Huang, A. Kwok, C. Follonier, C. Deng, and R. Scully. 2014. BRCA1 controls homologous recombination at Tus/Ter-stalled mammalian replication forks. *Nature.* 510:556–559. https://doi.org/10.1038/nature13295

Willis, N.A., A. Panday, E.E. Duffey, and R. Scully. 2018. Rad51 recruitment and exclusion of non-homologous end joining during homologous recombination at a Tus/Ter mammalian replication fork barrier. *PLoS Genet.* 14:e1007486. https://doi.org/10.1371/journal.pgen.1007486

Ying, S., S. Minocherhomji, K.L. Chan, T. Palmai-Pallag, W.K. Chu, T. Wass, H.W. Mankouri, Y. Liu, and I.D. Hickson. 2013. MUS81 promotes common fragile site expression. *Nat. Cell Biol.* 15:1001–1007. https://doi.org/10.1038/ncb2773

Yokoyama, T., M. Yukuhiro, Y. Iwasaki, C. Tanaka, K. Sankoda, R. Fujiwara, A. Shibuta, T. Higashi, K. Motoyama, H. Arima, et al. 2019. Identification of candidate molecular targets of the novel antineoplastic antimitotic NP-10. *Sci. Rep.* 9:16825. https://doi.org/10.1038/s41598-019-53259-2

Zhang, J., and J.C. Walter. 2014. Mechanism and regulation of incisions during DNA interstrand cross-link repair. *DNA Repair (Amst.).* 19: 135–142. https://doi.org/10.1016/j.dnarep.2014.03.018

Zhang, J.M., T. Yadav, J. Ouyang, L. Lan, and L. Zou. 2019. Alternative Lengthening of Telomeres through Two Distinct Break-Induced Replication Pathways. *Cell Rep.* 26:955–968.e3. https://doi.org/10.1016/j.celrep.2018.12.102

JCB

Supplemental material

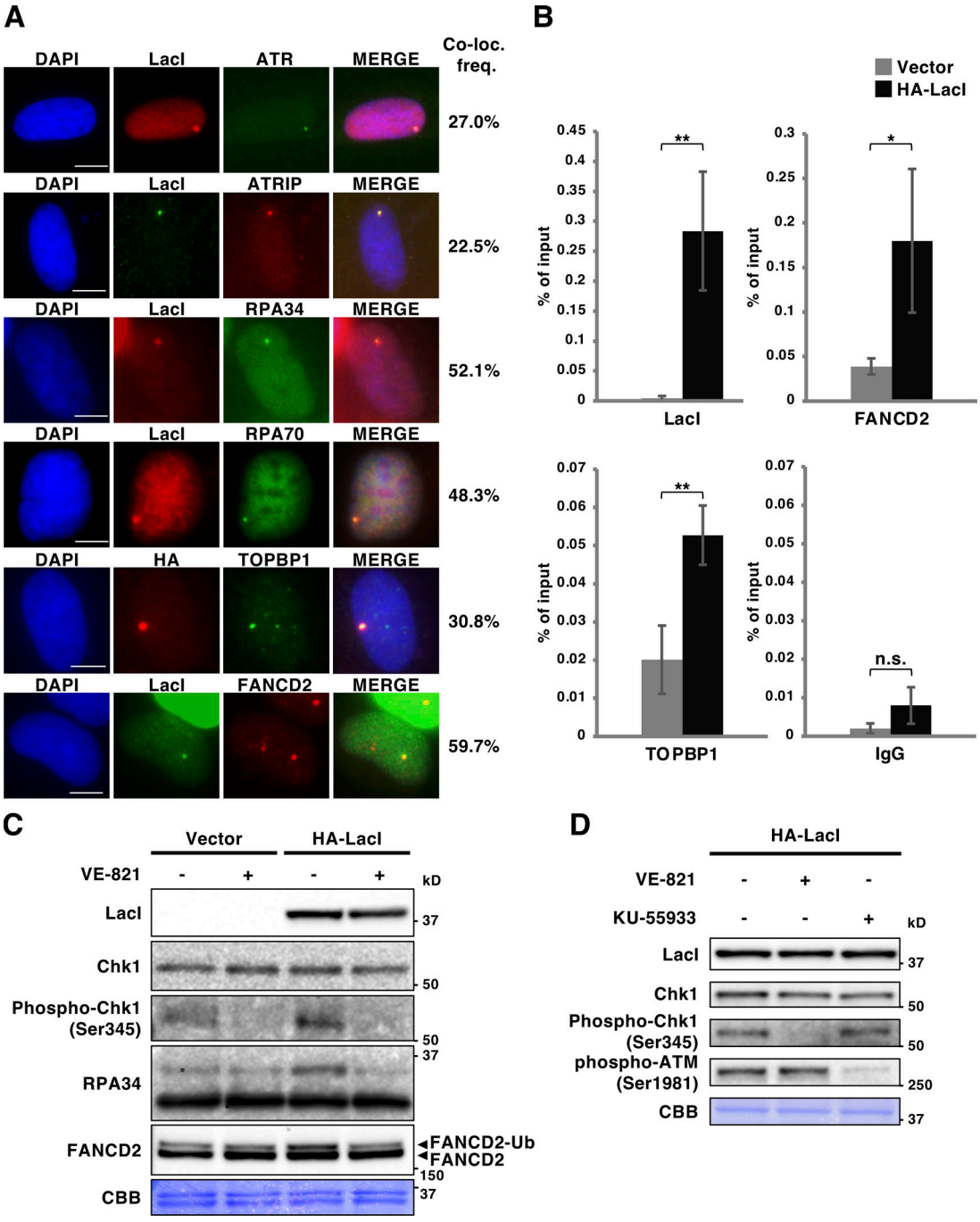

Figure S1. **Recruitment of various DDR proteins to *lacO* arrays after transient expression of HA-LacI in U2OS 2–6-3 cells. (A)** U2OS 2–6-3 cells were transfected with HA-LacI expression vector for 24 h using Lipofectamine 2000 reagent (Invitrogen) and then double immunostained with the indicated antibodies, followed by DAPI staining. Representative images and colocalization frequencies (%) of DDR-protein foci with LacI foci are shown. Values were calculated from the sum scores of at least two independent experiments. Scale bars, 10 µm. **(B)** U2OS 2–6-3 cells were transfected with the empty or the HA-LacI expression vectors for 24 h and then subjected to ChIP–quantitative PCR analysis with the indicated antibodies. Quantitative PCR was performed with primer pairs to detect *lacO* sequences. Results are shown as the percentage of input DNA. Means ± SD are shown (n = 4). *, $P < 0.05$; **, $P < 0.01$; n.s., not significant (two-tailed Student's t test). **(C and D)** U2OS 2–6-3 cells transfected as in (B) were treated with 10 µM VE-821 (ATR/ATM inhibitor), 10 µM KU-55933 (ATM inhibitor), or a control vehicle (DMSO) for 6 h and then subjected to immunoblotting. Data are representative of two or more independent experiments. In this experimental condition, VE-821 selectively inhibited ATR-mediated phosphorylation of Chk1 (Ser345), but not autophosphorylation of ATM (Ser1981). CBB, Coomassie Brilliant Blue; FANCD2-Ub, monoubiquitinated FANCD2.

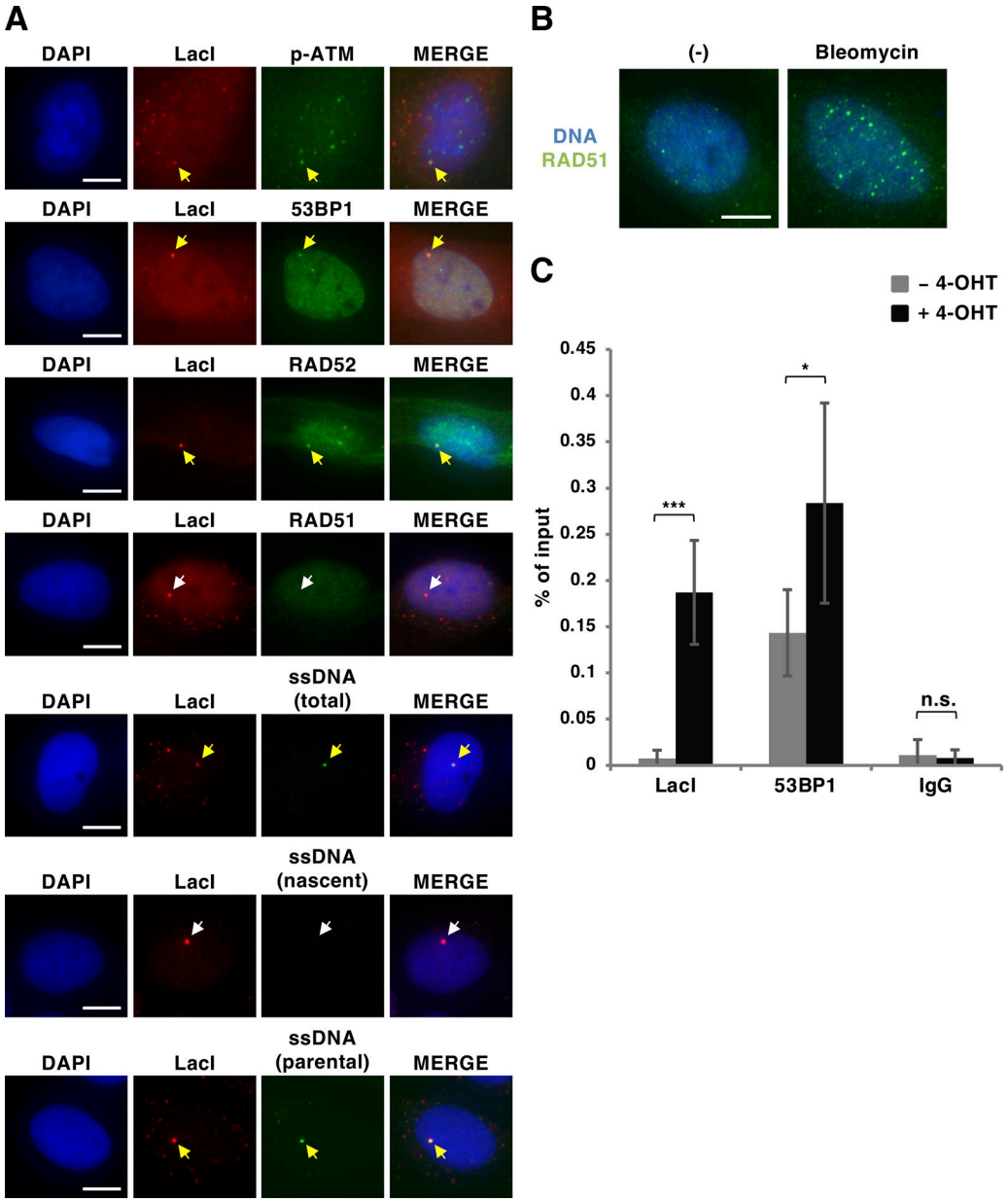

Figure S2. **Recruitment of various DDR proteins to *lacO* arrays in U2OS 40–2-6 ER-LacI cells. (A)** U2OS 40–2-6 ER-LacI cells treated with 1 µM 4-OHT for 2 h were double immunostained with the indicated antibodies and counterstained with DAPI. ssDNA was stained with anti-BrdU antibody under nondenaturing conditions. For detection of total ssDNA, DNA was labeled for 24 h with 10 µM BrdU. For detection of nascent-strand ssDNA, newly synthesized DNA was labeled with BrdU during treatment with 4-OHT. For detection of parental-strand ssDNA, DNA was labeled with 10 µM BrdU for 20 h, followed by a chase in fresh medium without BrdU for 2 h before addition of 4-OHT. Representative images are shown, and the colocalization frequencies are shown in Fig. 1 D. Yellow arrows indicate colocalization of DDR proteins with the foci of HA-LacI, and white arrows indicate noncolocalization. Scale bars, 10 µm. **(B)** The antibody used in this study can detect bleomycin-induced RAD51 foci. U2OS 40–2-6 ER-LacI cells were treated with 8 µM Bleomycin for 18 h, then immunostained with anti-RAD51 antibody, followed by DAPI staining. Representative images are shown. Scale bar, 10 µm. **(C)** U2OS 40–2-6 ER-LacI cells treated with 1 µM 4-OHT or a control vehicle (EtOH) for 2 h were subjected to ChIP-quantitative PCR analysis using the indicated antibodies. Enrichment of the *lacO* sequences is shown as the percent of input DNA. Means ± SD are shown (n = 6 for control rabbit IgG; n = 7 for LacI and 53BP1). *, P < 0.05; ***, P < 0.001; n.s., not significant (two-tailed Student's t test).

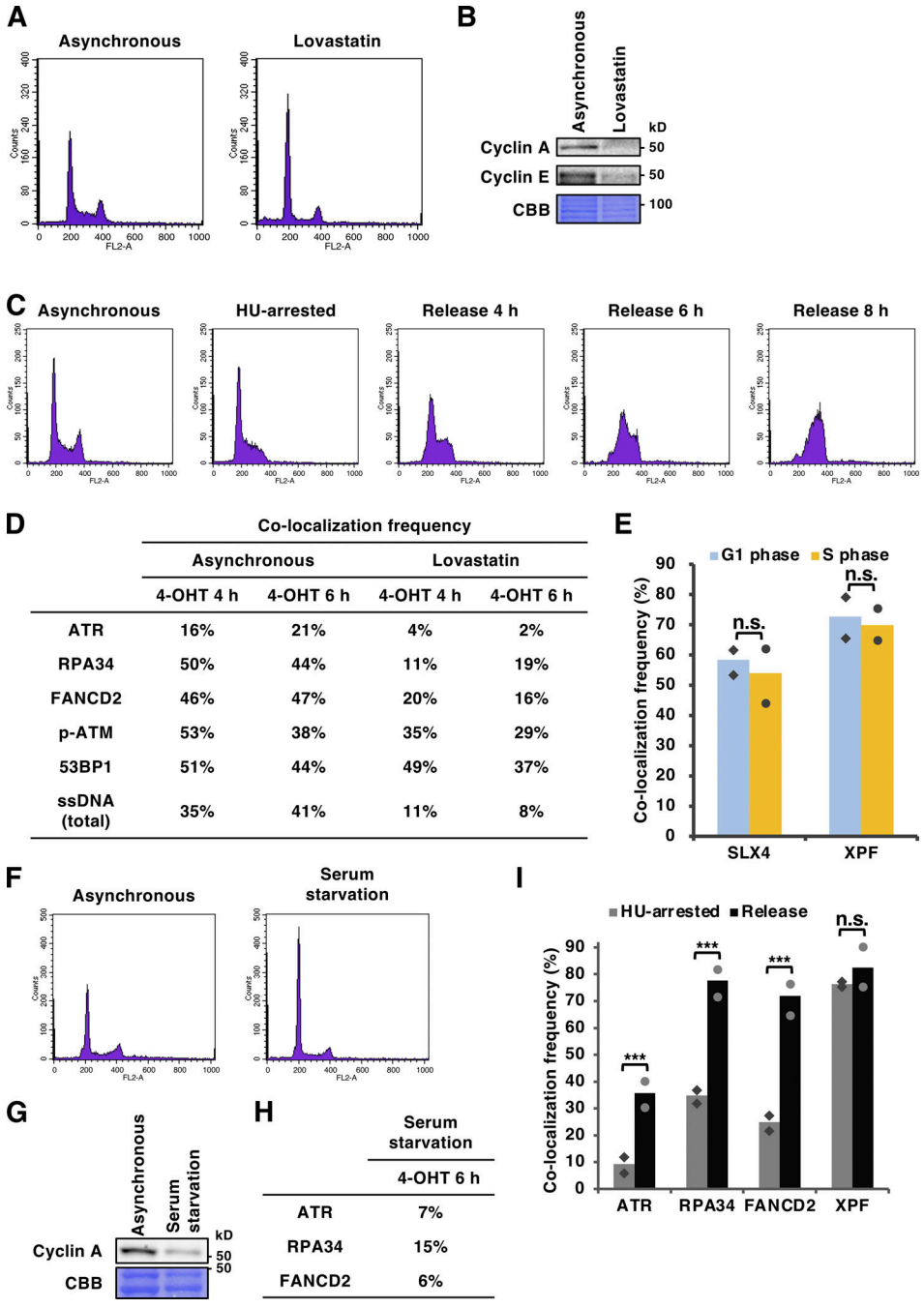

Figure S3. **Cell-cycle synchronization of U2OS 40–2-6 ER-LacI cells and the effect of synchronization on the DDRs induced by LacI. (A and B)** G1-phase synchronization. U2OS 40–2-6 ER-LacI cells were treated with 40 µM lovastatin for 40 h and then subjected to FACS (A) and SDS-PAGE followed by immunoblotting (B). Coomassie Brilliant Blue staining served as the loading control. G1 synchronization was confirmed by the reduction in cyclin A and cyclin E protein levels (B). Data are representative of two independent experiments. **(C)** S-phase synchronization. U2OS 40–2-6 ER-LacI cells were synchronized with 2.5 mM HU for 18 h and released into fresh medium. Cell-cycle distribution was analyzed by flow cytometry at the indicated times after release. Data are representative of two independent experiments. **(D)** Asynchronous cells or G1-synchronized cells as described in (A) were treated with 1 µM 4-OH-tamoxifen (4-OHT) for 4 h or 6 h. Colocalization frequencies of the indicated foci with LacI foci were analyzed as described in Fig. 1 E. **(E)** U2OS 40–2-6 ER-LacI cells were synchronized in G1 phase or in S phase as described in Fig. 1 E, treated with 1 µM 4-OHT for 2 h, and double immunostained, followed by DAPI staining. Colocalization frequencies of the indicated foci were calculated from the sum scores of two independent experiments. n.s., not significant (χ^2 test). Individual data points from the two independent experiments are also presented. **(F–H)** G0-phase synchronization. Cells synchronized at G0 phase by serum starvation (0.1% FCS) for 72 h were subjected to FACS analysis (F) and immunoblotting for cyclin A (G). In G0 cells, cyclin A levels were reduced. After 72 h serum starvation, cells were treated with 1 µM 4-OHT for 6 h, and the colocalization frequencies of the indicated DDR factors with LacI were analyzed (H). Compared with the values with asynchronous cells (e.g., those shown in D), the accumulation frequencies were lower. **(I)** Cells arrested in early S phase as described in C were treated with 1 µM 4-OHT and either left arrested with HU or released into fresh medium for 6 h. Colocalization frequencies were calculated from the sum scores of two independent experiments. ***, $P < 0.001$; n.s., not significant (χ^2 test). Individual data points from the two independent experiments are also shown. CBB, Coomassie Brilliant Blue.

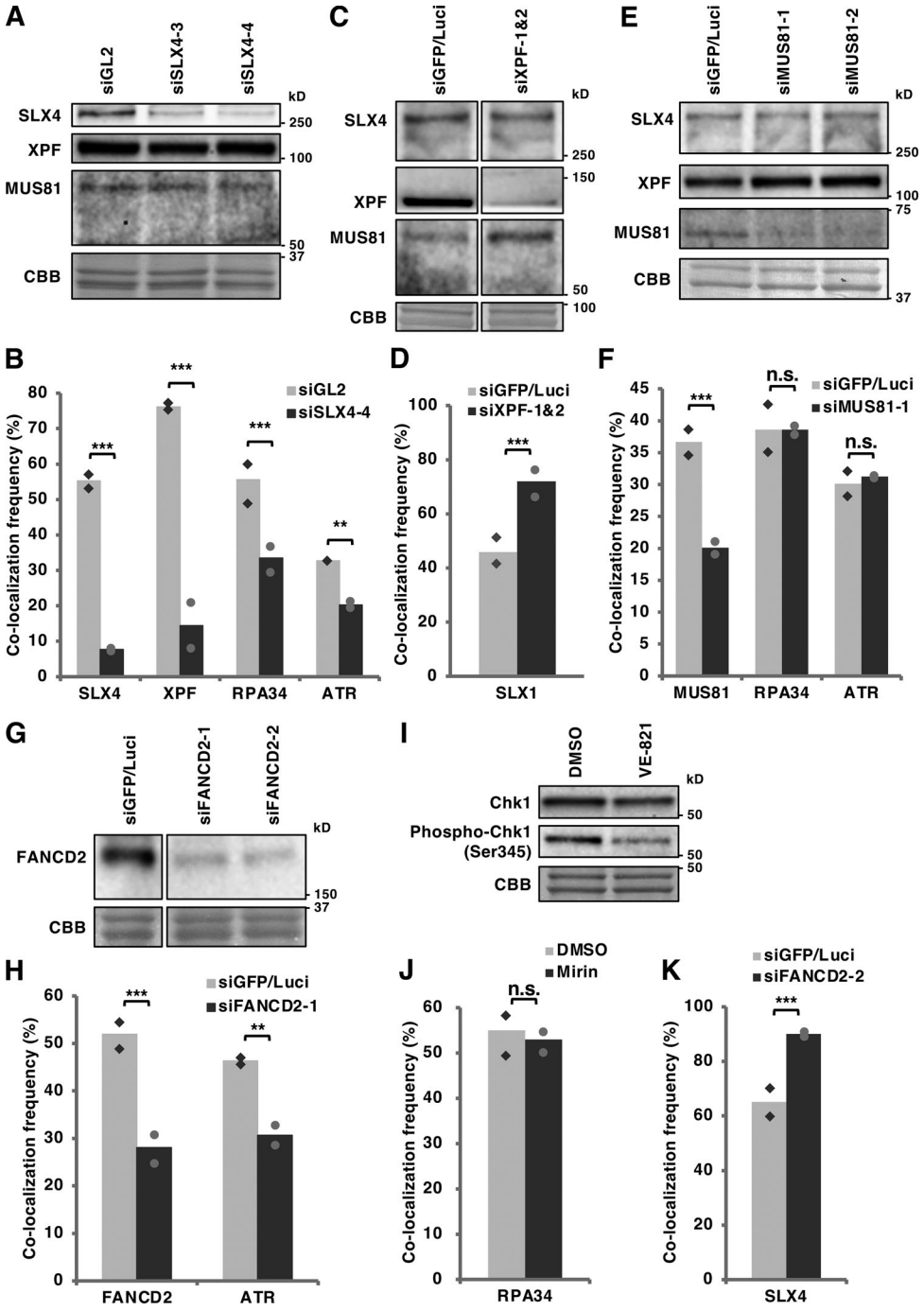

Figure S4. **Silencing of SLX4, XPF, MUS81, and FANCD2, and additional data for SLX4- and FANCD2-mediated accumulation of the DDR factors at the LacI-bound *lacO*. (A and B)** U2OS 40–2-6 ER-LacI cells were transfected with control (siGL2) or SLX4 (siSLX4-3 or siSLX4-4)–targeting siRNAs for 48 h. **(A)** Confirmation of SLX4 knockdown. Cells were subjected to SDS-PAGE and immunoblotting with the indicated antibodies. Coomassie Brilliant Blue staining served as a loading control. **(B)** After siRNA treatment, cells were further treated with 1 µM 4-OHT for 2 h and then subjected to colocalization analysis as described in Fig. 1, C and D. Values were calculated from the sum scores of two independent experiments. **, $P < 0.01$; ***, $P < 0.001$ (χ^2 test). Individual data points from the two independent experiments are also shown. **(C–F)** Cells were transfected with control siRNAs (a mixture of siGFP and siLuci) or siRNAs targeting XPF (siXPF-1 and siXPF-2) or MUS81 (siMUS81-1 or siMUS81-2) for 48 h and analyzed as described in A and B. ***, $P < 0.001$; n.s., not significant (χ^2 test). **(G and H)** Cells were transfected with control (mixture of siGFP and siLuci) or FANCD2 (siFANCD2-1 or siFANCD2-2)-targeting siRNAs for 48 h. **(G)** Cells were then subjected to immunoblotting with anti-FANCD2 antibody. **(H)** At 42 h after siRNA transfection, cells were treated with 1 µM 4-OHT for 6 h and then subjected to colocalization analysis as described in B. **, $P < 0.01$; ***, $P < 0.001$ (χ^2 test). **(I)** U2OS 40–2-6 ER-LacI cells were treated with 10 µM ATR inhibitor (VE-821) or a vehicle (DMSO) for 6 h and 1 µM 4-OHT for the last 2 h (as in Fig. 3 E). Cells were then subjected to SDS-PAGE and immunoblotting to confirm that ATR-mediated Chk1 phosphorylation is inhibited by VE-821 treatment. **(J)** U2OS 40–2-6 ER-LacI cells were incubated with 1 µM 4-OHT and either DMSO as a vehicle or 50 µM mirin for 2 h. Colocalization frequencies of RPA foci with LacI foci are analyzed as described in B. n.s., not significant (χ^2 test). **(K)** U2OS 40–2-6 ER-LacI cells were transfected with the indicated siRNAs. At 42 h after siRNA transfection, cells were treated with 1 µM 4-OHT for a further 6 h and then analyzed as described in B. ***, $P < 0.001$ (χ^2 test).